

# Anisotropic Green Coordinates

DONG XIAO, University of Science and Technology of China, China  
 RENJIE CHEN\*, University of Science and Technology of China, China  
 BAILIN DENG, Cardiff University, UK

We live in a world filled with anisotropy, a ubiquitous characteristic of both natural and engineered systems. In this study, we concentrate on space deformation and introduce *anisotropic Green coordinates*, which provide versatile effects for cage-based and variational deformations in both two and three dimensions. The anisotropic Green coordinates are derived from the anisotropic Laplacian equation  $\nabla \cdot (A \nabla u) = 0$ , where  $A$  is a symmetric positive definite matrix. This equation belongs to the class of constant-coefficient second-order elliptic equations, exhibiting properties analogous to the Laplacian equation but incorporating the matrix  $A$  to characterize anisotropic behavior. Based on this equation, we establish the boundary integral formulation, which is subsequently discretized to derive anisotropic Green coordinates defined on the vertices and normals of oriented simplicial cages. Our method satisfies basic properties such as linear reproduction and translation invariance, and possesses closed-form expressions for both 2D and 3D scenarios. We also give an intuitive geometric interpretation of the approach, demonstrating that our method generates a quasi-conformal mapping. Furthermore, we derive the gradients and Hessians of the deformation coordinates and employ the local-global optimization framework to facilitate variational shape deformation, enabling flexible shape manipulation while achieving as-rigid-as-possible shape deformation. Experimental results demonstrate that anisotropic Green coordinates offer versatile and diverse deformation options, providing artists with enhanced flexibility and introducing a novel perspective on spatial deformation.

**CCS Concepts:** • Computing methodologies → Shape modeling; Geometric deformation.

**Additional Key Words and Phrases:** Anisotropic deformation, Green coordinates, Cage-based deformation, Variational shape deformation

## 1 Introduction

Space deformation is a basic problem in geometric modeling. Instead of directly modifying the object surface, space deformation treats the surface as an embedding in the ambient space and deforms the space through deformation handles [Ben-Chen et al. 2009]. Cage-based deformation is a typical example in which the embedded object deforms according to the manipulation of the cage [Ströter et al. 2024]. For each point  $\eta$  within the cage, a series of functions  $\phi_i(\eta)$  is constructed for each cage vertex  $v_i$ . These functions satisfy the partition of unity property,  $\sum_{i=1}^n \phi_i(\eta) = 1$ , and the linear reproduction property  $\eta = \sum_{i=1}^n \phi_i(\eta) v_i$ . The functions  $\phi_i(\eta)$  are commonly called the Generalized Barycentric Coordinates (GBC) [Floater 2015; Hormann and Sukumar 2017].

GBC is usually interpolatory and expresses the point inside the cage as an affine sum of the cage vertices. Although it demonstrates

good consistency with the target cage, it introduces obvious shearing artifacts, particularly when the cage undergoes affine transformations [Lipman et al. 2008]. In practice, it is also desirable for the deformed object to maintain a certain degree of conformality with the original object. Based on the Green's third identity of harmonic functions, Lipman et al. [2008] propose Green coordinates, which take into account both the cage vertices  $v_i$  and the cage normals  $n_j$ . Green coordinates satisfy  $\eta = \sum_{i=1}^n \phi_i(\eta) v_i + \sum_{j=1}^m \psi_j(\eta) n_j$  for  $\eta$  inside the cage. These coordinates enable shape-preserving deformations, characterized by angle-preserving in 2D and quasi-conformality in 3D. However, conformality is a strict and absolute condition, which also restricts the deformation diversity of Green coordinates once the source and target cages are fixed. In practical applications and artistic design, there is often a demand for more flexible and versatile deformation styles, which can be achieved through adjusting various parameters. In the real world, materials such as bones, wood, and fibers exhibit anisotropic structures, prompting users to seek deformations that are more “flexible” or more “rigid” along specific directions.

Based on previous observations, we propose to incorporate the anisotropic property into the traditional Green coordinates. The Laplacian operator is the composition of divergence and gradient, i.e.,  $\Delta = \nabla \cdot \nabla$ . Therefore, we can introduce anisotropy within the divergence operator and consider the anisotropic Laplacian equation  $\nabla \cdot (A \nabla u) = 0$ , where  $A$  is a positive-definite matrix. The matrix  $A$  introduces varying scales in different directions, thereby incorporating anisotropic properties in the formulation. Furthermore, the anisotropic Laplacian equation also gives rise to corresponding boundary integral formulation and leads to the anisotropic Green's identity, which form the foundation for constructing the anisotropic Green coordinates. We show that anisotropic Green coordinates satisfy linear reproduction and translation invariance properties, and produce versatile deformation results with varying control matrices  $A$ . Additionally, we provide closed-form expressions for both 2D and 3D cases and offer intuitive geometric interpretations of the method. We also relate the distortion of the deformation mapping to the condition number of  $A$ , and mathematically demonstrate that anisotropic Green coordinates exhibit quasi-conformal properties. Through extensive experiments, we validate that anisotropic Green coordinates provide artists with a broader range of deformation options and enhance the diversity of deformations choices. Moreover, appropriate selection of the matrix  $A$  enables desired effects, such as tighter adherence to the deformed cage or reduced isotropic and area distortion.

To further demonstrate the broad applicability of the closed-form anisotropic Green coordinates, we also derive their gradients and Hessians and perform variational shape deformation [Ben-Chen et al. 2009], which minimizes energy functional of the deformation

\*Corresponding author

Authors' Contact Information: Dong Xiao, xiaodong@ustc.edu.cn, School of Mathematical Sciences, University of Science and Technology of China, China; Renjie Chen, renjiec@ustc.edu.cn, School of Mathematical Sciences, University of Science and Technology of China, China; Bailin Deng, dengb3@cardiff.ac.uk, School of Computer Science and Informatics, Cardiff University, UK.

map. This approach enables flexible control through space constraints and supports the as-rigid-as-possible deformation strategy. The incorporation of anisotropy further extends the applicability of the variational shape deformation framework to a wider range of scenarios.

## 2 Related Work

### 2.1 Cage-based Deformation

Cage-based deformation is a fundamental topic in geometry processing, where users manipulate a coarse control structure to drive the deformation of complex objects within the enclosed space [Ströter et al. 2024]. Two critical factors in this problem are the geometry of the cage structure and the deformation coordinates defined on the cage. The most commonly used cage structure is the oriented simplicial surface, such as closed polygonal chains in 2D and triangle meshes in 3D [Ben-Chen et al. 2009; Ju et al. 2005; Lipman et al. 2008; Thiery et al. 2024; Weber et al. 2012; Yan and Schaefer 2019]. It is the first-order approximation of co-dimensional one surfaces. Other methods utilize high-order surfaces, such as polynomial or Bézier surfaces, as the cage structure [Li et al. 2013; Lin and Chen 2024; Liu et al. 2024; Michel et al. 2025; Michel and Thiery 2023; Qin et al. 2024; Wu et al. 2025; Xiao and Chen 2025]. Such structures enable more precise and flexible control over curved and bending deformations.

While the cage structure can influence the flexibility, the deformation effect is predominantly determined by the specific deformation coordinates established on the cage. The most widely utilized methods are generalized barycentric coordinates (GBC), which formulate interpolatory coordinates as a partition of unity and can accurately represent an arbitrary point  $\eta$  within the cage. As pioneering works, Floater [2003], Floater et al. [2005], and Ju et al. [2005] construct closed-form mean value coordinates by projecting the enclosing cage onto a sphere centered at  $\eta$  and calculating the contribution of each cage vertex based on this spherical projection. There are also other techniques for constructing GBC, such as using the Laplacian equation [Joshi et al. 2007], Poisson integral formula [Li and Hu 2013], probability theory [Chang et al. 2023; Hormann and Sukumar 2008], or stochastic sampling and Monte Carlo integration [de Goes and Desbrun 2024]. Additionally, transfinite coordinates [Belyaev 2006; Chang and Hormann 2025; Dyken and Floater 2009] extend the concept of traditional discrete barycentric coordinates to continuous boundaries, offering a general theoretical framework.

In addition to barycentric coordinates, some other deformation coordinates consider both the cage vertices and cage normals, and therefore achieve shape-preserving deformations. Shape preservation means that the deformed shape maintains a certain degree of conformality with the original shape and avoids large shearing artifacts. The typical methods are the Green coordinates [Lipman and Levin 2009; Lipman et al. 2008; Thiery and Boubekeur 2022; Wu et al. 2025; Xiao and Chen 2025], which utilize Green's third identity to establish the deformation formulation and naturally satisfy linear reproduction and transformation invariance. Other techniques involve Cauchy coordinates [Lin and Chen 2024; Liu et al. 2025b; Weber et al. 2009], which is demonstrated to be geometrically equivalent to Green coordinates in the planar domain.

However, the deformation effects of Green coordinates and Cauchy coordinates are fixed. Specifically, once the source and target cages are determined, the deformation is uniquely defined. To address this limitation, some approach solve the biharmonic Dirichlet problem, which incorporates gradient variations into the formulation [Liu et al. 2025a; Thiery et al. 2024; Weber et al. 2012]. Alternatively, Somigliana coordinates [Chen et al. 2023] generalize Green coordinates based on the Navier–Cauchy equation of linear elasticity. This approach enables physically plausible volume control while preserving similarity invariance. However, it lacks a closed-form solution and requires a CUDA-dependent implementation. Another option is to use variational deformation techniques to optimize the deformation map, as discussed in the following subsection.

### 2.2 Variational Shape Deformation

Variational methods are widely used in formulating partial differential equations for practical problems, such as the minimal surface equation [Pinkall and Polthier 1993]. They address the most fundamental problem in functional analysis of finding a function  $f$  that minimizes the energy functional  $E(f)$ . Ben-Chen et al. [2009] introduce the variational harmonic map in space deformation, which defines  $E(f)$  based on Green coordinates, enabling deformation control with space constraints and as-rigid-as-possible properties. The optimization problem is solved through a local-global minimization strategy [Liu et al. 2008; Sorkine and Alexa 2007], which requires computing the Jacobian and Hessian of Green coordinates. Subsequent research has extended this technique by incorporating various coordinate systems or employing higher-order cage structures [Liu et al. 2025b; Michel et al. 2025; Thiery et al. 2024; Weber et al. 2012; Wu et al. 2025]. Additionally, Dodik et al. [2023] introduce variational barycentric coordinates, a neural field-based framework that optimizes generalized barycentric coordinates by minimizing their total variation.

### 2.3 Anisotropy in Geometry Processing

Anisotropy is a fundamental phenomenon in both natural systems and physical processes, playing an important role in simulating directionally dependent materials and generating adaptive computational domains. Research in this field encompasses theoretical foundations, numerical methodologies, and practical applications.

At the mathematical fundamental level, Owhadi and Zhang [2007] establish a metric-based upscaling framework for elliptic PDEs of the form  $\mathcal{L}u = \nabla \cdot (A(x)\nabla u(x))$  and rigorously analyze its mathematical properties within the Sobolev space. Kharevych et al. [2009] construct anisotropic elasticity tensors on coarse meshes through harmonic homogenization to preserve fine-scale directional properties. Kim et al. [2019] focus on anisotropic hyperelasticity and propose an anisotropic strain invariant for the inversion-safe energy model, complemented by a rehabilitation technique to address degenerate elements. Lin et al. [2024] derive the anisotropic as-rigid-as-possible energy for elastic materials and provide a robust formulation suitable for finite element simulations.

Anisotropy is also well introduced in mesh processing. Chen and Desbrun [2022] expand Green's functions by leveraging the anisotropic characteristics of general linear elastic materials, which

allows for real-time control of material deformation without volumetric discretization. Ren et al. [2018] propose generating planar anisotropic meshes for a given metric tensor and establishing a quasi-conformal mapping to transform the anisotropic metric into a Euclidean metric. Zhong et al. [2013] embed the anisotropic Riemannian metrics into higher-dimensional isotropic spaces, achieving efficient particle-based anisotropic meshing. Ma et al. [2025] derive the anisotropic Gauss formulation and utilize this boundary integral formulation for point cloud normal orientation and surface reconstruction. This work focuses on geometry topics that are distinct from our method and only considers the anisotropic equations in diagonal forms.

### 3 Anisotropic Green Coordinates

In this section, we present a detailed derivation of the anisotropic Green coordinates. We begin by introducing the boundary integral formulation of the anisotropic Laplacian equation. It is non-trivial that, despite the introduction of anisotropy, we can still use boundary integrals to determine the coordinates of any point within the cage. Subsequently, we discretize this identity to obtain anisotropic Green coordinates that exhibit linear reproduction and translation invariance. Then, we analyze their properties.

#### 3.1 Anisotropic Laplacian Equation

Green's third identity can be derived from the Laplacian equation  $\Delta u = 0$ , which serves as the foundation for establishing Green coordinates. Since  $\Delta = \nabla \cdot \nabla$ , we can introduce anisotropy within the divergence operator. Our method starts with the anisotropic Laplacian equation in  $\mathbb{R}^d$ ,  $d \geq 2$ , which is given by:

$$\nabla \cdot (A \nabla u(x)) = 0, \quad (1)$$

where  $A$  is a  $d \times d$  positive-definite matrix with constant coefficients. This equation is a special case of the second-order elliptic operator  $\mathcal{L}u = \nabla \cdot (A(x)\nabla u(x)) + b(x) \cdot \nabla u(x) + c(x)u(x)$ , and shares many similar properties with the classical Laplacian operator. When  $A$  is not constant, properties of solutions are generally studied in Sobolev spaces [Evans and Lawrence 1964], and obtaining explicit solutions is often challenging. Thus, we focus on the scenario where  $A$  is a constant-coefficient matrix, and both the convection-enhancing term  $b(x)$  and the first-order term  $c(x)$  are set to zero. It has been mathematically established that every differential operator  $\mathcal{L}$  with constant coefficients has a fundamental solution [Folland 1995].

We first introduce the concept of the square root of a positive definite matrix. It is known that every positive definite matrix  $A$  can be diagonalized as  $A = P \Lambda P^\top$ , where

$$\Lambda = \text{diag}(\lambda_1, \lambda_2, \dots, \lambda_d) \quad (2)$$

is a  $d$ -dimensional diagonal matrix with  $\lambda_i > 0$  for  $i = 1, 2, \dots, d$ , and  $P$  is an orthogonal matrix satisfying  $P^{-1} = P^\top$ . By expressing

$$\Lambda^{1/2} = \text{diag}(\sqrt{\lambda_1}, \sqrt{\lambda_2}, \dots, \sqrt{\lambda_d}), \quad (3)$$

we can define the square root of  $A$  as  $A^{1/2} = P \Lambda^{1/2} P^\top$ . It is then straightforward to verify that  $(A^{1/2})^2 = A$ .  $A^{1/2}$  is also symmetric and positive definite.

Next, we will present some theorems related to the anisotropic Laplacian equation. While we believe these properties have been

investigated in prior mathematical research, as they are closely related to the generalized Green's function [Chen and Kuo 2005], we are not aware of specific literature in the fields of cage or variational shape deformation that comprehensively addresses these results. Therefore, we provide a detailed discussion of them in the following.

**THEOREM 1.** *The fundamental solution of the anisotropic Laplacian Equation  $\nabla_\xi \cdot (A \nabla_\xi G_A(\xi, \eta)) = \delta(\xi - \eta)$  is:*

$$G_A(\xi, \eta) = \begin{cases} \frac{1}{2\pi\sqrt{\det A}} \log \sqrt{(\xi - \eta)^\top A^{-1}(\xi - \eta)}, & d = 2, \\ -\frac{1}{(d-2)\omega_d\sqrt{\det A}} [(\xi - \eta)^\top A^{-1}(\xi - \eta)]^{\frac{2-d}{2}}, & d \geq 3, \end{cases} \quad (4)$$

where  $\delta(x)$  is the Dirac delta distribution satisfying  $\delta(x) = 0$  for  $x \neq 0$  and  $\int_{\mathbb{R}^d} \delta(x) = 1$ , and  $\omega_d = 2\pi^{d/2}/\Gamma(d/2)$  represents the surface area of the unit sphere in  $\mathbb{R}^d$ .

**PROOF.** We begin with the variable substitutions  $x = A^{-1/2}\xi$  and  $y = A^{-1/2}\eta$ . According to Lemmas A.1 in the supplementary material, we have

$$\begin{aligned} \nabla_\xi \cdot (A \nabla_\xi u) &= \nabla_\xi \cdot (A A^{-1/2} \nabla_x u) = \nabla_\xi \cdot (A^{1/2} \nabla_x u) \\ &= \nabla_x \cdot (A^{-1/2} A^{1/2} \nabla_x u) = \Delta_x u. \end{aligned} \quad (5)$$

Since the Dirac delta distribution is a generalized function that violates the  $C^2$  condition of Lemma A.1, we introduce Lemma A.2 to establish the same variable substitution formula within the framework of distribution theory. Furthermore, within distribution theory, equality holds in the almost everywhere sense; thus, functions may differ on a set of measure zero. Nevertheless, for the fundamental solution, it is customary to seek a function that is smooth everywhere except at the singular point.

In the following, we denote by  $G(u) = G(x, y)$  the fundamental solution of the isotropic Laplacian equation  $\Delta_x G(x, y) = \delta(x - y)$ , where  $u = x - y$ , and by  $G_A(\xi, \eta)$  the fundamental solution of the anisotropic Laplacian equation  $\nabla_\xi \cdot (A \nabla_\xi G_A(\xi, \eta)) = \delta(\xi - \eta)$  with respect to  $A$ . According to Eq. (5), we know that  $G_A$  satisfying

$$\Delta_x G_A(x, y) = \delta(A^{1/2}(x - y)) = \frac{1}{\sqrt{\det A}} \delta(x - y). \quad (6)$$

The last equality follows from Lemma A.3 together with the identity  $\det A^{1/2} = |\det A^{1/2}| = \sqrt{\det A}$ . Therefore, we conclude that  $\sqrt{\det A} G_A(x - y)$  is the fundamental solution  $G(u)$  of  $d$ -dimensional isotropic Laplacian equation, which is given by

$$G(u) = \begin{cases} \frac{1}{2\pi} \log |u|, & d = 2, \\ -\frac{1}{(d-2)\omega_d} \frac{1}{|u|^{d-2}}, & d \geq 3. \end{cases} \quad (7)$$

Substituting  $u = x - y = A^{-1/2}(\xi - \eta)$  to  $G(u)$  and we complete the proof.  $\square$

Moreover, the gradient  $\nabla_\xi G_A(\xi, \eta)$  can be evaluated explicitly as:

$$\nabla_\xi G_A(\xi, \eta) = \begin{cases} \frac{1}{2\pi\sqrt{\det A}} [(\xi - \eta)^\top A^{-1}(\xi - \eta)]^{-1} A^{-1}(\xi - \eta), & d = 2, \\ \frac{1}{\omega_d\sqrt{\det A}} [(\xi - \eta)^\top A^{-1}(\xi - \eta)]^{-\frac{d}{2}} A^{-1}(\xi - \eta), & d \geq 3, \end{cases} \quad (8)$$

will also be used frequently in the subsequent analysis.

### 3.2 Construction of Anisotropic Green Coordinates

Before deriving the anisotropic Green coordinates, we first revisit the construction of the classical isotropic Green coordinates, which are defined on an oriented simplicial surface cage  $P = (\mathbb{V}, \mathbb{T})$  [Lipman and Levin 2009; Lipman et al. 2008], where  $\mathbb{V}$  denotes the cage vertices and  $\mathbb{T}$  represents the face normals. Green coordinates are constructed based on Green's third identity. Specifically, when  $\Omega$  is a bounded open set in  $\mathbb{R}^d$  with  $C^2$  boundary, and  $u(\eta)$  is a harmonic function on  $\overline{\Omega}$ , then for  $\eta \in \Omega$ , we have:

$$u(\eta) = \int_{\partial\Omega} u(\xi) \frac{\partial G}{\partial \mathbf{n}}(\xi, \eta) d\sigma_\xi - \int_{\partial\Omega} G(\xi, \eta) \frac{\partial u}{\partial \mathbf{n}}(\xi) d\sigma_\xi, \quad (9)$$

where  $G(\xi, \eta)$  is the fundamental solution of the isotropic Laplacian equation (7). The directional derivatives are taken along the outward normal.

*Remark:* The left hand side of Eq. (9) can be written as  $c(\eta)u(\eta)$  if  $\eta \in \mathbb{R}^d$  is not constrained in the open set  $\Omega$  and  $\partial\Omega$  is  $C^2$ . The coefficient  $c(\eta)$  satisfies  $c(\eta) = 1$  if  $\eta \in \Omega$ ,  $c(\eta) = 1/2$  if  $\eta \in \partial\Omega$ , and  $c(\eta) = 0$  if  $\eta \in \mathbb{R}^d \setminus \overline{\Omega}$ . We ignore the boundary continuity condition for discrete inputs when  $\eta \in \Omega$ .

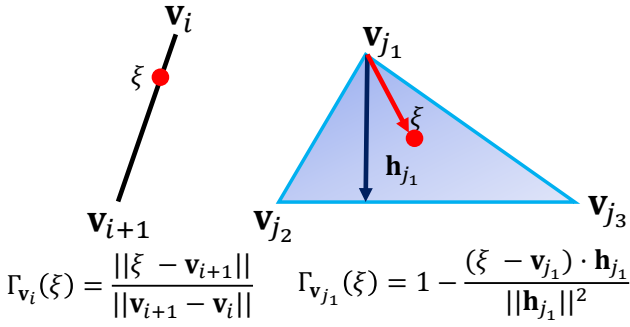


Fig. 1. Illustration of the hat function in 2D and 3D.

Given the cage  $P = (\mathbb{V}, \mathbb{T})$ , we can use above identity to reproduce any point  $\eta$  inside the cage using the vertices  $\{v_i | i \in I_{\mathbb{V}}\}$  and outward normals  $\{\mathbf{n}_j | j \in I_{\mathbb{T}}\}$  of the cage boundary as follows:

$$\eta = F(\eta, P) = \sum_{i \in I_{\mathbb{V}}} \phi_i(\eta) v_i + \sum_{j \in I_{\mathbb{T}}} \psi_j(\eta) \mathbf{n}_j, \quad \eta \in \Omega, \quad (10)$$

where

$$\phi_i(\eta) = \int_{\xi \in \mathcal{N}\{v_i\}} \Gamma_{v_i}(\xi) \frac{\partial G}{\partial \mathbf{n}}(\xi, \eta) d\sigma_\xi, \quad i \in I_{\mathbb{V}}, \quad (11)$$

$$\psi_j(\eta) = - \int_{\xi \in \mathcal{E}_j} G(\xi, \eta) d\sigma_\xi, \quad j \in I_{\mathbb{T}}. \quad (12)$$

In the above formulations,  $I_{\mathbb{V}}$  and  $I_{\mathbb{T}}$  represent the index set of the cage vertices and faces, respectively;  $\mathcal{N}\{v_i\}$  represents the faces adjacent to  $v_i$ , and  $\Gamma_{v_i}(\xi)$  is a piecewise linear hat function, which takes the value one at  $v_i$ , zero at all other vertices, and varies linearly across each face within  $\mathcal{N}\{v_i\}$ . As illustrated in Fig. 1, the explicit form of  $\Gamma_{v_i}(\xi)$  in the 2D case is given by  $\Gamma_{v_i}(\xi) = \frac{\|\xi - v_{i+1}\|}{\|v_{i+1} - v_i\|}$ .

In the 3D scenario,  $\Gamma_{v_{j1}}(\xi)$  is expressed as  $\Gamma_{v_{j1}}(\xi) = 1 - \frac{(\xi - v_{j1}) \cdot h_{j1}}{\|h_{j1}\|^2}$ , where  $h_{j1}$  denotes the altitude corresponding to the edge opposite

$v_{j1}$ . Furthermore,  $\Gamma_{v_{j1}}(\xi)$  essentially represents the barycentric coordinate of  $\xi$  relative to  $v_{j1}$  within  $\Delta v_{j1} v_{j2} v_{j3}$ . That is,  $\xi = \Gamma_{v_{j1}}(\xi) v_{j1} + \Gamma_{v_{j2}}(\xi) v_{j2} + \Gamma_{v_{j3}}(\xi) v_{j3}$  and  $\Gamma_{v_{j1}}(\xi) + \Gamma_{v_{j2}}(\xi) + \Gamma_{v_{j3}}(\xi) = 1.0$ .

When the source cage  $P$  is deformed to the target cage  $\tilde{P}$ , the new location  $\tilde{\eta}$  of  $\eta$  is computed as:

$$\tilde{\eta} = F(\eta, \tilde{P}) = \sum_{i \in I_{\mathbb{V}}} \phi_i(\eta) \tilde{v}_i + \sum_{j \in I_{\mathbb{T}}} \psi_j(\eta) s_j \tilde{\mathbf{n}}_j, \quad (13)$$

where  $\tilde{v}_i$  and  $\tilde{\mathbf{n}}_j$  denote the vertices and normals of the deformed cage, respectively. Throughout this work, the tilde symbol is used to represent quantities associated with the deformed value or target cage. The scale factor  $s_j$  preserves scale invariance in 2D and quasiconformality in 3D, as detailed in Section 3 of [Lipman et al. 2008].

Next, we derive the anisotropic boundary integral formulation of the anisotropic Laplacian equation, which establishes the mathematical foundation for our anisotropic Green coordinates.

**THEOREM 2.** *If  $\Omega$  is a bounded open set in  $\mathbb{R}^d$  with  $C^2$  boundary, and  $u(\xi)$  is a  $C^2$  scalar function satisfying  $\nabla \cdot (\mathbf{A} \nabla u(\xi)) = 0$  on  $\overline{\Omega}$ , where  $\mathbf{A}$  is symmetric positive definite. Then, for  $\eta \in \Omega$ , we have*

$$u(\eta) = \int_{\partial\Omega} u(\xi) (\mathbf{A} \nabla G_{\mathbf{A}}(\xi, \eta) \cdot \mathbf{n}(\xi)) d\sigma_\xi - \int_{\partial\Omega} G_{\mathbf{A}}(\xi, \eta) (\mathbf{A} \nabla u(\xi) \cdot \mathbf{n}(\xi)) d\sigma_\xi, \quad (14)$$

where  $G_{\mathbf{A}}(\xi, \eta)$  is the fundamental solution of the anisotropic Laplacian equation  $\nabla_\xi \cdot (\mathbf{A} \nabla_\xi G_{\mathbf{A}}(\xi, \eta)) = \delta(\xi - \eta)$ , and  $\mathbf{n}(\xi)$  the outward normal of  $\partial\Omega$  at  $\xi$ .

**PROOF.** We begin the proof by applying the divergence theorem. Let  $\Omega$  be a bounded open set in  $\mathbb{R}^d$  and  $\mathbf{F}$  is a  $C^2$  vector-valued function defined on the closure  $\overline{\Omega}$ . Then,

$$\int_{\Omega} \nabla \cdot \mathbf{F} dV = \int_{\partial\Omega} \mathbf{F} \cdot \mathbf{n} d\sigma, \quad (15)$$

where  $\mathbf{n}$  is the normal vector of  $\partial\Omega$ . Let  $\mathbf{F} = u(\mathbf{A} \nabla v)$ , where  $u, v$  are two scalar functions on  $\overline{\Omega}$ . By applying the rule for computing the divergence of function products, we obtain the following equation:

$$\nabla \cdot \mathbf{F} = \nabla u \cdot (\mathbf{A} \nabla v) + u \nabla \cdot (\mathbf{A} \nabla v). \quad (16)$$

Combining Eqs. (15) and (16), we get

$$\int_{\Omega} \nabla u \cdot (\mathbf{A} \nabla v) + u \nabla \cdot (\mathbf{A} \nabla v) dV = \int_{\partial\Omega} u (\mathbf{A} \nabla v \cdot \mathbf{n}) d\sigma. \quad (17)$$

Exchanging  $u$  and  $v$  in the above equation and obtain

$$\int_{\Omega} \nabla v \cdot (\mathbf{A} \nabla u) + v \nabla \cdot (\mathbf{A} \nabla u) dV = \int_{\partial\Omega} v (\mathbf{A} \nabla u \cdot \mathbf{n}) d\sigma. \quad (18)$$

Then, we can subtract Eq. (18) from Eq. (17). Since  $\mathbf{A}$  is symmetric,

$$\nabla u \cdot (\mathbf{A} \nabla v) = \nabla u^\top \mathbf{A} \nabla v = \nabla u^\top \mathbf{A}^\top \nabla v = (\mathbf{A} \nabla u)^\top \nabla v = \nabla v \cdot (\mathbf{A} \nabla u), \quad (19)$$

Therefore, we have

$$\int_{\Omega} u \nabla \cdot (\mathbf{A} \nabla v) - v \nabla \cdot (\mathbf{A} \nabla u) dV = \int_{\partial\Omega} u (\mathbf{A} \nabla v \cdot \mathbf{n}) - v (\mathbf{A} \nabla u \cdot \mathbf{n}) d\sigma. \quad (20)$$

Let  $v(\xi) = G_A(\xi, \eta)$ , where  $\eta \in \Omega$  is fixed, and the integral is taken with respect to the variable  $\xi$ . Then,  $\nabla \cdot (\mathbf{A} \nabla v(\xi)) = \delta(\xi - \eta)$ , and we have

$$\int_{\Omega} u(\xi) \nabla \cdot (\mathbf{A} \nabla G_A(\xi, \eta)) dV_{\xi} = \int_{\Omega} u(\xi) \delta(\xi - \eta) dV_{\xi} = u(\eta). \quad (21)$$

Consequently, when  $u$  satisfies  $\nabla \cdot (\mathbf{A} \nabla u(\xi)) = 0$ , we obtain Equation (14) and complete the proof.  $\square$

*Remark:* From a strict mathematical perspective, the proof above remains not rigorous enough, as  $G_A$  is singular at  $\xi = \eta$  when performing the volume integration. The standard approach is to excise  $B_{\epsilon}(\eta)$  centered at  $\eta$  and let  $\epsilon \rightarrow 0$ , or to construct a sequence of functions that converges pointwise to the fundamental solution while remaining free of singularities (replacing  $\|\xi - \eta\|$  with  $(\|\xi - \eta\|^2 + \epsilon^2)^{1/2}$ ). Here, however, we prove the result directly in the sense of distributions.

We can derive the anisotropic Green coordinates with the natural linear reproduction property by setting  $u(\eta) = \eta$  in Eq. (14). There is a remark that  $u$  is a scalar function in Eq. (14). However, we can apply the identity to each coordinate component separately. Specifically, let  $u_k(\eta) = \eta_k$ , which returns the  $k$ -th component of  $\eta = (\eta_1, \eta_2, \dots, \eta_d)^T$ . Moreover, denote  $\mathbf{A} = (\mathbf{a}_1, \mathbf{a}_2, \dots, \mathbf{a}_d)$ , where  $\mathbf{a}_k$  is the  $k$ -th column of  $\mathbf{A}$ . Then,  $\mathbf{A} \nabla u_k(\xi) \cdot \mathbf{n}(\xi) = (\mathbf{a}_k)^T \mathbf{n}(\xi)$ . We can then combine the  $d$  components to obtain  $\eta = (u_1(\eta), \dots, u_d(\eta))^T$ . Moreover, the composed normal term on the right-hand side is  $\mathbf{A}^T \mathbf{n}_j = \mathbf{A} \mathbf{n}_j$ . Considering the boundary integration region as the cage boundary, we have the following equations:

$$\begin{aligned} \eta &= \sum_{j \in I_{\mathbb{T}}} \left( \int_{t_j} \xi (\mathbf{A} \nabla G_A(\xi, \eta) \cdot \mathbf{n}(\xi)) d\sigma_{\xi} - \int_{t_j} G_A(\xi, \eta) \mathbf{A} \mathbf{n}(\xi) d\sigma_{\xi} \right) \\ &= \sum_{j \in I_{\mathbb{T}}} \sum_{\mathbf{v}_i \in \mathbb{V}(t_j)} \mathbf{v}_i \left( \int_{t_j} \Gamma_i(\xi) \mathbf{A} \nabla G_A(\xi, \eta) \cdot \mathbf{n}(\xi) d\sigma_{\xi} \right) \\ &\quad - \sum_{j \in I_{\mathbb{T}}} \mathbf{A} \mathbf{n}_j \left( \int_{t_j} G_A(\xi, \eta) d\sigma_{\xi} \right), \end{aligned} \quad (22)$$

where  $I_{\mathbb{T}}$  denotes the index set of the cage faces, and  $\mathbb{V}(t_j)$  represents the vertex set of  $t_j$ . By rearranging the above equation, the anisotropic Green coordinates can be expressed as:

$$\eta = \sum_{i \in I_{\mathbb{V}}} \phi_i^A(\eta) \mathbf{v}_i + \sum_{j \in I_{\mathbb{T}}} \psi_j^A(\eta) \mathbf{A} \mathbf{n}_j, \quad \eta \in \Omega, \quad (23)$$

where

$$\phi_i^A(\eta) = \int_{\xi \in N\{\mathbf{v}_i\}} \Gamma_i(\xi) \mathbf{A} \nabla G_A(\xi, \eta) \cdot \mathbf{n}(\xi) d\sigma_{\xi}, \quad i \in I_{\mathbb{V}}, \quad (24)$$

$$\psi_j^A(\eta) = - \int_{\xi \in t_j} G_A(\xi, \eta) d\sigma_{\xi}, \quad j \in I_{\mathbb{T}}. \quad (25)$$

Compared to the traditional Green coordinates (Eqs (10) to (12)), the integral expressions of  $\phi_i^A(\eta)$  and  $\psi_j^A(\eta)$  are now related to  $G_A(\xi, \eta)$  instead of  $G(\xi, \eta)$ . Moreover, the Neumann term of Eq. (23), which is constructed based on the cage normals, now becomes  $\mathbf{A} \mathbf{n}_j$ . When the source cage is deformed to  $\tilde{\mathbf{P}}$  with new vertices  $\tilde{\mathbf{v}}_i$  and face normals  $\tilde{\mathbf{n}}_j$ , the deformed position  $\tilde{\eta}$  of  $\eta$  is given by:

$$\tilde{\eta} = \sum_{i \in I_{\mathbb{V}}} \phi_i^A(\eta) \tilde{\mathbf{v}}_i + \sum_{j \in I_{\mathbb{T}}} \psi_j^A(\eta) s_j \mathbf{A} \tilde{\mathbf{n}}_j, \quad (26)$$

where  $s_j$  is the scale factor analogous to that in [Lipman et al. 2008]. A detailed discussion of this term will be provided in the following subsection.

### 3.3 Properties

To analyze the deformation properties of the anisotropic Green coordinates, we first revisit the properties of the isotropic case, as examined in [Lipman and Levin 2009; Lipman et al. 2008]. Specifically, these properties include: (1) Linear reproduction:  $\eta = F(P, \eta)$  for  $\eta \in \Omega$ ; (2) Translation invariance:  $\sum_{i \in I_{\mathbb{V}}} \phi_i(\eta) = 1$  for  $\eta \in \Omega$ ; (3) Rotation and scale invariance: for an affine transformation  $T$ ,  $T\eta = F(\eta, TP)$ ; (4) Shape preservation: the deformation is angle-preserving in 2D and quasi-conformal in 3D; and (5) Smoothness:  $\phi_i(\eta)$  and  $\psi_j(\eta)$  are  $C^{\infty}$  for  $\eta \in \Omega$ . We observe that the anisotropic Green coordinates retain the properties of linear reproduction, translation invariance, scale invariance, quasi-conformality and smoothness. However, it does not satisfy the rotation invariance. Additionally, in 2D, these coordinates are not angle-preserving but exhibit quasi-conformality.

**Linear reproduction:** The anisotropic boundary integral formula naturally satisfies the linear reproduction property. As shown in Eq. (26), when the source and target cages are identical and  $s_j = 1$ , substituting the coordinate expressions back yields Eq. (22), verifying that  $\tilde{\eta} = \eta$ .

**Translation invariance:** Translation invariance follows from the fact that  $\phi_i^A(\eta)$  satisfies the partition of unity property, i.e.,  $\sum_{i \in I_{\mathbb{V}}} \phi_i^A(\eta) = 1$ . This property can be proven by setting  $u(\eta) = 1$  in Eq. (14), which yields:

$$\int_{\partial\Omega} (\mathbf{A} \nabla G_A(\xi, \eta) \cdot \mathbf{n}(\xi)) d\sigma_{\xi} = 1, \quad \eta \in \Omega. \quad (27)$$

Furthermore,  $\Gamma_{\mathbf{v}_i, t_j}(\eta)$  in the expression for  $\phi_i^A(\eta)$  is actually the barycentric coordinates of  $\mathbf{v}_i$  with respect to  $t_j$ . Therefore,

$$\begin{aligned} \sum_{i \in I_{\mathbb{V}}} \phi_i^A(\eta) &= \sum_{j \in I_{\mathbb{T}}} \sum_{\mathbf{v}_i \in \mathbb{V}(t_j)} \left( \int_{t_j} \Gamma_{\mathbf{v}_i, t_j}(\xi) (\mathbf{A} \nabla G_A(\xi, \eta) \cdot \mathbf{n}(\xi)) d\sigma_{\xi} \right) \\ &= \int_{\partial\Omega} (\mathbf{A} \nabla G_A(\xi, \eta) \cdot \mathbf{n}(\xi)) d\sigma_{\xi} = 1. \end{aligned} \quad (28)$$

**Scale and rotation invariance** Anisotropic Green coordinates do not necessarily satisfy rotation invariance, as  $\mathbf{T}$  and  $\mathbf{A}$  are not necessarily commutative when  $\mathbf{T}$  is an arbitrary rotation matrix. Regarding the selection of the scaling factor  $s_j$  in Eq. (26) for scale invariance, Green coordinates [Lipman et al. 2008] establish a simplex  $S_j$  formed by  $t_j$  and  $\mathbf{v}_{j_1} + \mathbf{n}_j$ , and  $\tilde{S}_j$  formed by  $\tilde{t}_j$  and  $\tilde{\mathbf{v}}_{j_1} + \tilde{\mathbf{n}}_j$ , where  $\mathbf{v}_{j_1}$  is a vertex of  $t_j$ . The scaling factor  $s_j$  in Eq. (26) is derived by analyzing the stretch of the face to ensure that  $T(S_j)$  is similar to  $\tilde{S}_j$ , resulting in  $s_j = \|T\|_2$ , where  $T$  represents the scale transformation. In the anisotropic scenario, the simplex is formed by  $t_j$  and  $\mathbf{v}_{j_1} + \mathbf{A} \mathbf{n}_j$ , as well as  $\tilde{t}_j$  and  $\tilde{\mathbf{v}}_{j_1} + s_j \mathbf{A} \tilde{\mathbf{n}}_j$ , respectively. To ensure that  $T(S_j)$  approximates  $\tilde{S}_j$  in shape, we can similarly conclude that  $s_j = \|T\|_2$ . Following the approach proposed by Lipman et al. [2008], we define  $s_j$  as follows. In the 2D case,  $s_j$  is given by the ratio of the deformed edge length to the original edge length, i.e.,  $s_j = \|\tilde{t}_j\| / \|t_j\|$ . For the

3D scenario, the scaling factor is defined as:

$$s_j = \sqrt{\frac{\sigma_1^2 + \sigma_2^2}{2}} = \frac{\sqrt{\|\tilde{u}\|^2\|\tilde{v}\|^2 - 2(\tilde{u} \cdot \tilde{v}) + \|\tilde{v}\|^2\|\tilde{u}\|^2}}{\sqrt{8\text{area}(t_j)}}, \quad (29)$$

where  $\sigma_1$  and  $\sigma_2$  denote the singular values of the linear map that transforms  $t_j$  to  $\tilde{t}_j$  when restricted to a plane. Moreover,  $u, v$  and  $\tilde{u}, \tilde{v}$  represent the edge vectors of  $t_j$  and  $\tilde{t}_j$ , respectively.

**Quasi-conformality** Although anisotropic Green coordinates are not strictly conformal in two dimensions, their quasi-conformality in both 2D and 3D can be established through the analysis of their relationship with the isotropic formulation presented in Section 5. Consequently, we also include the analysis of quasi-conformality in Section 5.

**Smoothness and generalized harmonicity** We also have the property that  $\phi_i^A(\eta)$  and  $\psi_j^A(\eta)$  are smooth for  $\eta \in \Omega$ . The reason is that  $G_A(\xi, \eta)$  is an elementary function with respect to  $\eta$  and has no singularities within the integration domain as  $\xi \neq \eta$ . Consequently,  $\phi_i^A(\eta)$  and  $\psi_j^A(\eta)$  are also smooth with respect to  $\eta$ , as they are obtained through differentiation and integration of  $G_A(\xi, \eta)$  with respect to  $\xi$ , and  $\Gamma_i(\xi)$  is independent of  $\eta$ . Moreover, we also conclude that  $\nabla_\eta \cdot (A\nabla_\eta \phi_i^A(\eta)) = 0$  and  $\nabla_\eta \cdot (A\nabla_\eta \psi_j^A(\eta)) = 0$ . We call this property **generalized harmonic with respect to A**. This can be briefly proven as follows: Due to the smoothness of  $G_A(\xi, \eta)$  when  $\xi \neq \eta$ , differentiation with respect to  $\eta$  can be interchanged with the integration with respect to  $\xi$ . Moreover, the gradient of  $G_A(\xi, \eta)$  with respect to  $\eta$  is simply the negative of its gradient with respect to  $\xi$ . Given that  $G_A(\xi, \eta)$  is generalized harmonic with respect to  $A$  in  $\xi$ , it is also generalized harmonic with respect to  $\eta$  in  $\Omega$ . It follows that  $\phi_i^A(\eta)$  and  $\psi_j^A(\eta)$  also inherit this property.

#### 4 Derivation of Closed-form Anisotropic Green Coordinates

We have derived the deformation formula for anisotropic Green coordinates and investigated its fundamental properties. In this section, we present closed-form expressions for  $\phi_i^A(\eta)$  and  $\psi_j^A(\eta)$  in both 2D and 3D. These analytical solutions are more accurate and computationally efficient compared to numerical methods for evaluating the integrals. In the following derivations, we frequently use formulations for the substitution of area elements on curves and surfaces embedded in  $\mathbb{R}^2$  and  $\mathbb{R}^3$ . These formulations are detailed in Lemmas A.4, A.5, and A.6 of the supplementary material. While these results do not rely on advanced mathematical concepts, they are non-trivial and not immediately obvious. Additionally, Appendix B provides a detailed derivation of the closed-form expressions for classical isotropic Green coordinates and their gradients and Hessians, which serve as the foundation for the anisotropic formulation.

##### 4.1 Closed-form Expressions for 2D Scenario

We begin by presenting the method in 2D. We assume that the 2D cage is a closed and oriented 1-mainfold in  $\mathbb{R}^2$  with vertices  $I_V = \{\mathbf{v}_i\}_{i=1}^N$  and faces  $I_T = \{f_j | f_j = \overrightarrow{\mathbf{v}_j \mathbf{v}_{j+1}}\}$  arranged in counter-clockwise order. We denote  $\mathbf{a}_j = \mathbf{v}_{j+1} - \mathbf{v}_j$ . Then, the unit outward normal  $\mathbf{n}_j$  of  $f_j$  is given by  $\mathbf{n}_j = \mathbf{a}_j^\perp / \|\mathbf{a}_j^\perp\|$ , where the superscript “ $\perp$ ” denotes the vector obtained by rotating the original vector 90

degrees clockwise. Then,  $\psi_j^A(\eta)$  has the following expression:

$$\psi_j^A(\eta) = - \int_{\xi \in f_j} G_A(\xi, \eta) d\sigma_\xi, \quad (30)$$

$$= \int_{\xi \in f_j} -\frac{1}{2\pi\sqrt{\det A}} \log \sqrt{(\xi - \eta)^\top A^{-1}(\xi - \eta)} d\sigma_\xi. \quad (31)$$

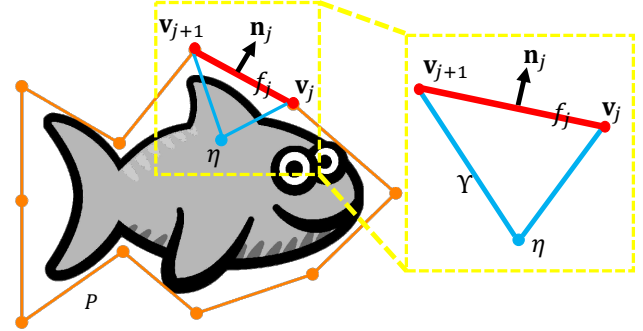


Fig. 2. The illustration of a 2D cage and its mathematical notations.

The key step is to transform the calculation of the anisotropic formulation into the isotropic one through the variable substitution. Specifically, let  $\mathbf{x} = A^{-1/2}\xi$ ,  $\mathbf{y} = A^{-1/2}\eta$ ,  $\mathbf{v}'_j = A^{-1/2}\mathbf{v}_j$  and  $\mathbf{v}'_{j+1} = A^{-1/2}\mathbf{v}_{j+1}$ . According to Lemma A.4 and Lemma A.5 of the supplementary material, we have  $d\sigma_\mathbf{x} = |\det A^{-1/2}| \|A^{1/2}\mathbf{n}_j\| d\sigma_\xi$ , where  $\mathbf{n}_j$  is the unit normal of  $f_j$ . Denoting  $f'_j = \overrightarrow{\mathbf{v}'_j \mathbf{v}'_{j+1}}$ , we have

$$\begin{aligned} \psi_j^A(\eta) &= \int_{\xi \in f_j} -\frac{1}{2\pi\sqrt{\det A}} \log \sqrt{(\xi - \eta)^\top A^{-1}(\xi - \eta)} d\sigma_\xi \\ &= \frac{1}{|\det A^{-1/2}| \|A^{1/2}\mathbf{n}_j\|} \int_{\xi \in f'_j} -\frac{1}{2\pi\sqrt{\det A}} \log \|\mathbf{x} - \mathbf{y}\| d\sigma_\mathbf{x} \\ &= \frac{1}{\sqrt{\mathbf{n}_j^\top A \mathbf{n}_j}} \int_{\xi \in f'_j} -\frac{1}{2\pi} \log \|\mathbf{x} - \mathbf{y}\| d\sigma_\mathbf{x}. \end{aligned} \quad (32)$$

According to [Lipman and Levin 2009], we can define  $\mathbf{a}_j = \mathbf{v}'_{j+1} - \mathbf{v}'_j$  and  $\mathbf{b}_j = \mathbf{v}'_j - \mathbf{y}$ . Then, the term  $\int_{\xi \in f'_j} \frac{1}{2\pi} \log \|\mathbf{x} - \mathbf{y}\| d\sigma_\mathbf{x}$  is equal to  $-\frac{\|\mathbf{a}_j\|}{4\pi} (Q(1) - Q(0))$ , where

$$\begin{aligned} Q(t) &= \left( t + \frac{\mathbf{a}_j \cdot \mathbf{b}_j}{\|\mathbf{a}_j\|^2} \right) \log (\|\mathbf{a}_j\|^2 t^2 + 2(\mathbf{a}_j \cdot \mathbf{b}_j) t + \|\mathbf{b}_j\|^2) \\ &\quad - \left( \frac{\|\mathbf{a}_j\|^2 + (\mathbf{a}_j \cdot \mathbf{b}_j)}{\|\mathbf{a}_j\|^2 \sqrt{\|\mathbf{a}_j\|^2 \|\mathbf{b}_j\|^2 - (\mathbf{a}_j \cdot \mathbf{b}_j)^2}} \right) \arctan \left( \frac{\|\mathbf{a}_j\|^2 t + (\mathbf{a}_j \cdot \mathbf{b}_j)}{\sqrt{\|\mathbf{a}_j\|^2 \|\mathbf{b}_j\|^2 - (\mathbf{a}_j \cdot \mathbf{b}_j)^2}} \right). \end{aligned} \quad (33)$$

Please refer to Appendix B.1 for more details on this formula.

We now proceed to the Dirichlet term  $\phi_{\mathbf{v}_j}^A(\eta)$ , which is obtained by summing the contributions over the edges associated with  $\mathbf{v}_i$ . We focus on the integral over a single edge  $f_j$ , denoted as  $\phi_{\mathbf{v}_j, f_j}^A(\eta)$ . Recall that  $\mathbf{x} = A^{-1/2}\xi$ ,  $\mathbf{y} = A^{-1/2}\eta$ ,  $\mathbf{v}'_j = A^{-1/2}\mathbf{v}_j$ ,  $\mathbf{v}'_{j+1} = A^{-1/2}\mathbf{v}_{j+1}$ ,  $f_j = \overrightarrow{\mathbf{v}_j \mathbf{v}_{j+1}}$  and  $f'_j = \overrightarrow{\mathbf{v}'_j \mathbf{v}'_{j+1}}$ . Let  $\Gamma_{\mathbf{v}_j, f_j}(\xi)$  be the hat-function of  $\xi$  with respect to  $\mathbf{v}_j$  in  $f_j$ , and  $\Gamma_{\mathbf{v}_j, f_j}(\mathbf{x})$  be the hat-function of  $\mathbf{x}$  with respect to  $\mathbf{v}'_j$  in  $f'_j$ . We first show that  $\Gamma_{\mathbf{v}_j, f_j}(\xi_0) = \Gamma_{\mathbf{v}'_j, f'_j}(\mathbf{x}_0)$  for

$\xi_0 \in f_j$  and  $\mathbf{x}_0 = \mathbf{A}^{-1/2} \xi_0$ . Recall that  $\Gamma_{\mathbf{v}_j, f_j}(\xi_0)$  is the barycentric coordinates of  $\xi_0$  with respect to  $\mathbf{v}_j$  in  $f_j$ , we obtain

$$\xi_0 = \Gamma_{\mathbf{v}_j, f_j}(\xi_0) \mathbf{v}_j + \Gamma_{\mathbf{v}_{j+1}, f_j}(\xi_0) \mathbf{v}_{j+1} \quad (34)$$

and

$$\Gamma_{\mathbf{v}_j, f_j}(\xi_0) + \Gamma_{\mathbf{v}_{j+1}, f_j}(\xi_0) = 1. \quad (35)$$

Then,

$$\begin{aligned} \mathbf{x}_0 &= \mathbf{A}^{-1/2} \xi = \Gamma_{\mathbf{v}_j, f_j}(\xi_0) \mathbf{A}^{-1/2} \mathbf{v}_j + \Gamma_{\mathbf{v}_{j+1}, f_j}(\xi_0) \mathbf{A}^{-1/2} \mathbf{v}_{j+1} \\ &= \Gamma_{\mathbf{v}_j, f_j}(\xi_0) \mathbf{v}'_j + \Gamma_{\mathbf{v}_{j+1}, f_j}(\xi_0) \mathbf{v}'_{j+1}. \end{aligned} \quad (36)$$

Therefore,  $\Gamma_{\mathbf{v}_j, f_j}(\xi_0)$ ,  $\Gamma_{\mathbf{v}_{j+1}, f_j}(\xi_0)$  and  $\Gamma_{\mathbf{v}'_j, f'_j}(\mathbf{x}_0)$ ,  $\Gamma_{\mathbf{v}'_{j+1}, f'_j}(\mathbf{x}_0)$  are both barycentric coordinates of  $\mathbf{x}_0$  in  $f'_j$ . As established in Lemma A.7, the barycentric coordinates of a simplex are uniquely determined due to the affine independence of its vertices. This property distinguishes them from barycentric coordinates in arbitrary polygonal domains, where uniqueness is generally not guaranteed. Therefore, we conclude that  $\Gamma_{\mathbf{v}_j, f_j}(\xi_0) = \Gamma_{\mathbf{v}'_j, f'_j}(\mathbf{x}_0)$  for any  $\xi_0 \in f_j$  and  $\mathbf{x}_0 = \mathbf{A}^{-1/2} \xi_0$ . Moreover, we have  $d\sigma_\xi = |\det \mathbf{A}^{1/2}| |\mathbf{A}^{-1/2} \mathbf{n}'_j| d\sigma_x$ , where  $\mathbf{n}'_j$  is the unit normal of  $\overrightarrow{\mathbf{v}'_j \mathbf{v}'_{j+1}}$ . Then, we can derive the closed-form solution of  $\phi_{\mathbf{v}_j, f_j}^A(\eta)$  as follows:

$$\begin{aligned} \phi_{\mathbf{v}_j, f_j}^A(\eta) &= \frac{1}{2\pi\sqrt{\det \mathbf{A}}} \int_{\xi \in f_j} \Gamma_{\mathbf{v}_j, f_j}(\xi) \frac{(\xi - \eta) \cdot \mathbf{n}_j}{(\xi - \eta)^\top \mathbf{A}^{-1}(\xi - \eta)} d\sigma_\xi \\ &= \frac{|\det \mathbf{A}^{1/2}| |\mathbf{A}^{-1/2} \mathbf{n}'_j|}{2\pi\sqrt{\det \mathbf{A}}} \int_{\mathbf{x} \in f'_j} \Gamma_{\mathbf{v}'_j, f'_j}(\mathbf{x}) \frac{\mathbf{A}^{1/2}(\mathbf{x} - \mathbf{y}) \cdot \left( \frac{\mathbf{A}^{-1/2} \mathbf{n}'_j}{\|\mathbf{A}^{-1/2} \mathbf{n}'_j\|} \right)}{(\mathbf{x} - \mathbf{y})^\top (\mathbf{x} - \mathbf{y})} d\mathbf{x} \\ &= \frac{1}{2\pi} \int_{\mathbf{x} \in f'_j} \Gamma_{\mathbf{v}'_j, f'_j}(\mathbf{x}) \frac{(\mathbf{x} - \mathbf{y}) \cdot \mathbf{n}'_j}{(\mathbf{x} - \mathbf{y})^\top (\mathbf{x} - \mathbf{y})} d\mathbf{x}. \end{aligned} \quad (37)$$

Denote  $\mathbf{a}_j = \mathbf{v}'_{j+1} - \mathbf{v}'_j$  and  $\mathbf{b}_j = \mathbf{v}'_j - \mathbf{y}$ . The term

$$\int_{\mathbf{x} \in f'_j} \Gamma_{\mathbf{v}'_j, f'_j}(\mathbf{x}) \frac{(\mathbf{x} - \mathbf{y}) \cdot \mathbf{n}'_j}{(\mathbf{x} - \mathbf{y})^\top (\mathbf{x} - \mathbf{y})} d\mathbf{x} \quad (38)$$

is equal to  $-\frac{\|\mathbf{a}_j\|(\mathbf{b}_j \cdot \mathbf{n}_j)}{2\pi} (W(1) - W(0))$ , where

$$\begin{aligned} W(t) &= \frac{1}{2\|\mathbf{a}_j\|^2} \log(\|\mathbf{a}_j\|^2 t^2 + 2t(\mathbf{a}_j \cdot \mathbf{b}_j) + \|\mathbf{b}_j\|^2) \\ &\quad - \left( \frac{\|\mathbf{a}_j\|^2 + (\mathbf{a}_j \cdot \mathbf{b}_j)}{\|\mathbf{a}_j\|^2 \sqrt{\|\mathbf{a}_j\|^2 \|\mathbf{b}_j\|^2 - (\mathbf{a}_j \cdot \mathbf{b}_j)^2}} \right) \arctan \left( \frac{\|\mathbf{a}_j\|^2 t + (\mathbf{a}_j \cdot \mathbf{b}_j)}{\sqrt{\|\mathbf{a}_j\|^2 \|\mathbf{b}_j\|^2 - (\mathbf{a}_j \cdot \mathbf{b}_j)^2}} \right). \end{aligned} \quad (39)$$

## 4.2 Closed-form Expressions for 3D Scenario

We can employ a similar methodology to derive the closed-form expression for the 3D case. Figure 3 depicts a tetrahedron formed by a triangular face  $t_j = \Delta \mathbf{v}_{j_1} \mathbf{v}_{j_2} \mathbf{v}_{j_3}$  of the cage and an interior point  $\eta$  within the cage. Let  $\mathbf{x} = \mathbf{A}^{-1/2} \xi$ ,  $\mathbf{y} = \mathbf{A}^{-1/2} \eta$ ,  $\mathbf{v}'_{j_1} = \mathbf{A}^{-1/2} \mathbf{v}_{j_1}$ ,  $\mathbf{v}'_{j_2} = \mathbf{A}^{-1/2} \mathbf{v}_{j_2}$  and  $\mathbf{v}'_{j_3} = \mathbf{A}^{-1/2} \mathbf{v}_{j_3}$ . According to Lemma A.6, we have  $d\sigma_x = |\det \mathbf{A}^{-1/2}| |\mathbf{A}^{1/2} \mathbf{n}_t| d\sigma_\xi$ , where  $\mathbf{n}_t$  denotes the unit outward normal vector of  $t_j$ . Furthermore, denoting  $t'_j = \Delta \mathbf{v}'_{j_1} \mathbf{v}'_{j_2} \mathbf{v}'_{j_3}$ , and its normal as  $\mathbf{n}'_t$ . Then, the Neumann term  $\psi_j^A(\eta)$  on  $t_j$  can be

computed as follows:

$$\begin{aligned} \psi_j^A(\eta) &= \int_{\xi \in t_j} \frac{1}{4\pi\sqrt{\det \mathbf{A}}} \frac{1}{(\xi - \eta)^\top \mathbf{A}^{-1}(\xi - \eta)} d\sigma_\xi \\ &= \frac{1}{|\det \mathbf{A}^{-1/2}| |\mathbf{A}^{1/2} \mathbf{n}_t|} \int_{\mathbf{x} \in t'_j} \frac{1}{4\pi\sqrt{\det \mathbf{A}}} \frac{1}{\|\mathbf{x} - \mathbf{y}\|} d\sigma_x \quad (40) \\ &= \frac{1}{\sqrt{\mathbf{n}_t^\top \mathbf{A} \mathbf{n}_t}} \int_{\mathbf{x} \in t'_j} \frac{1}{4\pi} \frac{1}{\|\mathbf{x} - \mathbf{y}\|} d\sigma_x. \end{aligned}$$

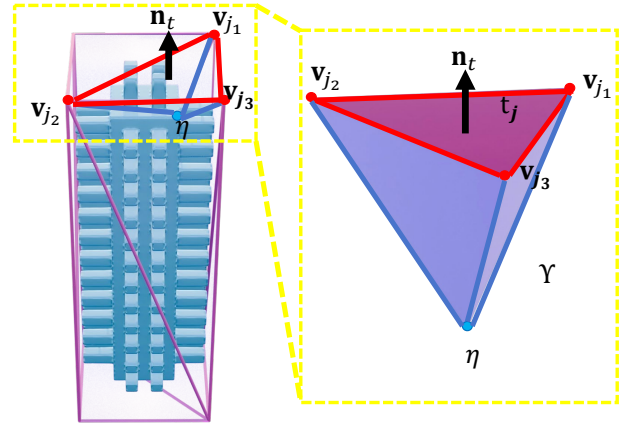


Fig. 3. A tetrahedron formed by a triangular face  $t_j = \Delta \mathbf{v}_{j_1} \mathbf{v}_{j_2} \mathbf{v}_{j_3}$  of a cage and the query point  $\eta$ .

For the Dirichlet term, we denote by  $\phi_{\mathbf{v}_{j_1}, t_j}^A(\eta)$  the contribution of  $t_j$  to  $\phi_{\mathbf{v}_{j_1}}^A(\eta)$ . According to Lemma A.6, we have  $d\sigma_\xi = |\det \mathbf{A}^{1/2}| |\mathbf{A}^{-1/2} \mathbf{n}'_t| d\sigma_x$ . Based on the uniqueness of the barycentric coordinates of a simplex (Lemma A.7), it holds that  $\Gamma_{\mathbf{v}_{j_1}, t_j}(\xi_0) = \Gamma_{\mathbf{v}'_{j_1}, t'_j}(\mathbf{x}_0)$  for  $\xi_0 \in t_j$  and  $\mathbf{x}_0 = \mathbf{A}^{-1/2} \xi_0$ . Therefore,

$$\begin{aligned} \phi_{\mathbf{v}_{j_1}, t_j}^A(\eta) &= \frac{1}{4\pi\sqrt{\det \mathbf{A}}} \int_{\xi \in t_j} \Gamma_{\mathbf{v}_{j_1}, t_j}(\xi) \frac{(\xi - \eta) \cdot \mathbf{n}_t}{[(\xi - \eta)^\top \mathbf{A}^{-1}(\xi - \eta)]^{\frac{3}{2}}} d\sigma_\xi \\ &= \frac{|\det \mathbf{A}^{1/2}| |\mathbf{A}^{-1/2} \mathbf{n}'_t|}{4\pi\sqrt{\det \mathbf{A}}} \int_{\mathbf{x} \in t'_j} \Gamma_{\mathbf{v}'_{j_1}, t'_j}(\mathbf{x}) \frac{\mathbf{A}^{1/2}(\mathbf{x} - \mathbf{y}) \cdot \left( \frac{\mathbf{A}^{-1/2} \mathbf{n}'_t}{\|\mathbf{A}^{-1/2} \mathbf{n}'_t\|} \right)}{[(\mathbf{x} - \mathbf{y})^\top (\mathbf{x} - \mathbf{y})]^{\frac{3}{2}}} d\mathbf{x} \\ &= \frac{1}{4\pi} \int_{\mathbf{x} \in t'_j} \Gamma_{\mathbf{v}'_{j_1}, t'_j}(\mathbf{x}) \frac{(\mathbf{x} - \mathbf{y}) \cdot \mathbf{n}'_t}{[(\mathbf{x} - \mathbf{y})^\top (\mathbf{x} - \mathbf{y})]^{\frac{3}{2}}} d\mathbf{x}. \end{aligned} \quad (41)$$

Then, we transform the computation of the anisotropic formulation into an isotropic one. The calculation of 3D isotropic Green coordinates is somewhat complex, and we provide the details in Appendix B.2 of the supplementary material. These derivations are primarily based on the findings of [Ben-Chen et al. 2009] and [Urago 2000], but we provide a more comprehensive derivation.

## 5 Discussion

In this section, we mainly derive the geometric interpretation of anisotropic Green coordinates in comparison to the isotropic counterparts, and demonstrate the quasi-conformality of our method. Furthermore, we emphasize the essential value of addressing problems from an anisotropic perspective.

We have the following observation when ignoring the effect of the scale factor  $s_j$ : the two approaches below are equivalent:

- (1) Given an input, first apply a global multiplication by  $\mathbf{A}^{-1/2}$  to the source cage, target cage, and the object; subsequently deform the object using the isotropic Green coordinates; and finally multiply globally by  $\mathbf{A}^{1/2}$ .
- (2) Employ the anisotropic Green coordinates for the source and target cages.

We will present the derivation of this equivalence subsequently. Despite the equivalence, we believe that there are still important points to illustrate the value of deriving the anisotropic Green coordinates. First, our method provides a geometric interpretation of Green's identity derived from the anisotropic Laplace equation. Second, as deformation coordinates, they need to be expressed as functions relative to the original cage, rather than the cage has undergone a global transformation. Moreover, when performing the variational method for deformation control (which will be presented in Section 6), it is more intuitive to analyze directly from the closed-form anisotropic formulation as well as its gradient and Hessian. Most importantly, during user interaction, the deformation coordinates  $\phi_i^A(\eta)$  and  $\psi_j^A(\eta)$  typically need to be calculated only once for the input source cage, and subsequent deformations do not require recalculation. If calculated directly using anisotropic Green coordinates, according to Eq. (26), only  $s_j$ ,  $\mathbf{A}\tilde{\mathbf{n}}_j$  and  $\tilde{\eta}$  are required to be computed every time. In contrast, if calculated from the perspective of the global transform, it is necessary to first compute the transformed target cage and normals, which increases the computational overhead. Furthermore, this study introduces a new perspective on cage-based and variational deformation. If the matrix  $\mathbf{A}$  can be optimized, there is potential to further enhance the practical value of the method, which remains a direction for our future work.

Next, we refer to the deformation effect obtained by “globally multiplying by  $\mathbf{A}^{-1/2}$ , performing deformation using isotropic Green coordinates, and then globally multiplying by  $\mathbf{A}^{1/2}$ ”, as *similarity Green deformation*. The name stems from the fact that this process closely resembles a matrix similarity transformation. We denote the vertices and normals of the cage as  $\{\mathbf{v}_i\}_{i=1}^N$  and  $\{\mathbf{n}_j\}_{j=1}^M$ . Moreover, we use the prime operator to denote the globally transformed values, e.g.,  $\mathbf{v}'_i = \mathbf{A}^{-1/2}\mathbf{v}_i$ ,  $\mathbf{n}'_j = \frac{\mathbf{A}^{1/2}\mathbf{n}_j}{\|\mathbf{A}^{1/2}\mathbf{n}_j\|}$ . Then, we can express the globally transformed values in terms of isotropic Green coordinates as:

$$\eta' = \sum_{i \in I_{V'}} \phi'_i(\eta') \mathbf{v}'_i + \sum_{j \in I_{T'}} \psi'_j(\eta') \mathbf{n}'_j. \quad (42)$$

The derivation of section 4.2 (Eqs. (32) and (37)) shows that  $\phi'_i(\eta') = \phi_i^A(\eta)$  and  $\psi'_j(\eta') = \|\mathbf{A}^{1/2}\mathbf{n}_j\| \psi_j^A(\eta)$ , where  $\mathbf{n}_j$  is the normal of  $f_j$ . Moreover, we have  $\eta = \mathbf{A}^{1/2}\eta'$ . Then,

$$\begin{aligned} \eta &= \mathbf{A}^{1/2}\eta' = \mathbf{A}^{1/2} \left( \sum_{i \in I_{V'}} \phi'_i(\eta') \mathbf{v}'_i + \sum_{j \in I_{T'}} \psi'_j(\eta') \mathbf{n}'_j \right) \\ &= \mathbf{A}^{1/2} \left( \sum_{i \in I_{V'}} \phi_i^A(\eta) \mathbf{A}^{-1/2} \mathbf{v}_i + \|\mathbf{A}^{1/2}\mathbf{n}_j\| \sum_{j \in I_{T'}} \psi_j^A(\eta) \frac{\mathbf{A}^{1/2}\mathbf{n}_j}{\|\mathbf{A}^{1/2}\mathbf{n}_j\|} \right) \\ &= \sum_{i \in I_{V'}} \phi_i^A(\eta) \mathbf{v}_i + \sum_{j \in I_{T'}} \psi_j^A(\eta) \mathbf{A} \mathbf{n}_j, \end{aligned} \quad (43)$$

and we show the equivalence between the anisotropic Green deformation and the similarity Green deformation.

Moreover, we can use the above analysis to demonstrate the quasi-conformality of our method. We denote the anisotropic deformation mapping as  $f_A(\eta)$ , and the corresponding isotropic mapping as  $f'(\eta)$ . Then,

$$f_A(\eta) = \mathbf{A}^{1/2} f'(\mathbf{A}^{-1/2}\eta). \quad (44)$$

The Jacobian of  $f_A(\eta)$  is given by:

$$J_{f_A}(\eta) = \mathbf{A}^{1/2} J_{f'}(\mathbf{A}^{-1/2}\eta) \mathbf{A}^{-1/2}, \quad (45)$$

where  $J_{f'}$  is the Jacobian of the isotropic formulation. Let  $K_A(\eta)$  denote the ratio of the maximum to the minimum singular values of the anisotropic deformation mapping, and  $K'(\eta)$  the corresponding isotropic ratio. Then,

$$\begin{aligned} K_A(\eta) &= \frac{\sigma_{\max}(J_{f_A}(\eta))}{\sigma_{\min}(J_{f_A}(\eta))} = \text{cond}(J_{f_A}(\eta)) \\ &= \text{cond}(\mathbf{A}^{1/2} J_{f'}(\mathbf{A}^{-1/2}\eta) \mathbf{A}^{-1/2}) \\ &\leq \text{cond}(\mathbf{A}^{1/2}) \text{cond}(J_{f'}(\mathbf{A}^{-1/2}\eta)) \text{cond}(\mathbf{A}^{-1/2}) \\ &= \text{cond}(\mathbf{A}) K'(\mathbf{A}^{-1/2}\eta), \end{aligned} \quad (46)$$

where  $\sigma_{\max}(J_{f_A}(\eta))$  and  $\sigma_{\min}(J_{f_A}(\eta))$  represent the maximum and minimum singular values of  $J_{f_A}(\eta)$ , and  $\text{cond}(\mathbf{A})$  represents the condition number of  $\mathbf{A}$ . Therefore, when Green coordinates are conformal in 2D, anisotropic Green coordinates are quasi-conformal with  $K_A(\eta) \leq \text{cond}(\mathbf{A})$ . When Green coordinates are quasi-conformal in 3D with a distortion bound  $M$ , anisotropic Green coordinates are quasi-conformal in 3D with a bound  $\text{cond}(\mathbf{A}) \cdot M$ . Moreover, since  $\mathbf{A} = \mathbf{P}^\top \Lambda \mathbf{P}$ , the condition number  $\text{cond}(\mathbf{A})$  is precisely the ratio of the largest to the smallest eigenvalues of  $\Lambda$ .

## 6 Variational Shape Deformation of Anisotropic Green Coordinates

In this section, we derive the expressions for the derivatives of anisotropic Green coordinates, specifically the gradients and Hessians of  $\phi_i^A(\eta)$  and  $\psi_j^A(\eta)$ . These derivatives form the foundation for deformation control in the variational shape deformation framework introduced in Ben-Chen et al. [2009]. In this method, an energy functional is defined to determine the optimal deformation mapping that satisfies user-specified constraints while simultaneously balancing smoothness and as-rigid-as-possible transformations. Previous work also demonstrates that the introduction of anisotropy does not conflict with our desire for rigid transformations at specific positions [Lin et al. 2024].

For a simplicial surface cage with vertices  $\mathbb{V}$  and faces  $\mathbb{T}$ , we can define the deformation map  $f_{a,b}(\eta)$  as a linear combination of basis functions  $\phi_i^A(\eta)$  and  $\psi_j^A(\eta)$  based on the anisotropic Green coordinates as

$$f_{a,b}(\eta) = \sum_{v \in \mathbb{V}} \mathbf{a}_v \phi_v^A(\eta) + \sum_{t \in \mathbb{T}} \mathbf{b}_t \psi_t^A(\eta), \quad (47)$$

where  $\mathbf{b}_t = \mathbf{A} \mathbf{n}_t$ . Here,  $\mathbf{a}_v \in \mathbb{R}^d$  represents the piecewise-linear coefficients defined on the cage vertices, while  $\mathbf{n}_t \in \mathbb{R}^d$  denotes the piecewise-constant coefficients defined on the cage faces. To enlarge the deformation space,  $\mathbf{a}_v$  and  $\mathbf{b}_t$  are treated as independent variables

and optimized separately. Since  $\mathbf{A}$  is invertible, we can directly optimize  $\mathbf{b}_t$ , as  $\mathbf{n}_t$  can be easily computed through  $\mathbf{n}_t = \mathbf{A}^{-1}\mathbf{b}_t$ .

To perform variational shape deformation, it is necessary to compute the gradients and Hessians of  $\phi_i^A(\eta)$  and  $\psi_j^A(\eta)$ . The core idea is to apply Lemma A.1 from the supplementary material to transform the formulation into an isotropic form. For the computation of the isotropic formulation, please refer to Appendix B.

Let  $t_j$  be a face of the cage and  $t'_j$  its transformation via left-multiplication of vertices by  $\mathbf{A}^{-1/2}$ . For any point  $\eta_0$  on  $t_j$  with normal  $\mathbf{n}_j$ , let  $\mathbf{y}_0 = \mathbf{A}^{-1/2}\eta_0$  be the corresponding point in  $t'_j$ . Moreover, let  $\psi_{t_j}^A(\eta_0)$  denote the Neumann term of  $t_j$  for the anisotropic Green coordinates at  $\eta_0$ , while  $\psi_{t'_j}^A(\mathbf{y}_0)$  represents the Neumann term of  $t'_j$  for the isotropic formulation. Based on the derivations in Section 4.2, we obtain:

$$\psi_{t_j}^A(\eta_0) = \frac{1}{\sqrt{\mathbf{n}_j^\top \mathbf{A} \mathbf{n}_j}} \psi_{t'_j}^A(\mathbf{y}_0), \quad (48)$$

Therefore, according to Lemma A.1, the gradient  $\nabla_\eta \psi_{t_j}^A(\eta_0)$  and Hessian  $\mathbf{H}_\eta \psi_{t_j}^A(\eta_0)$  can be calculated as:

$$\begin{aligned} \nabla_\eta \psi_{t_j}^A(\eta_0) &= \frac{1}{\sqrt{\mathbf{n}_j^\top \mathbf{A} \mathbf{n}_j}} \mathbf{A}^{-1/2} \nabla_{\mathbf{y}} \psi_{t'_j}^A(\mathbf{y}_0), \\ \mathbf{H}_\eta \psi_{t_j}^A(\eta_0) &= \frac{1}{\sqrt{\mathbf{n}_j^\top \mathbf{A} \mathbf{n}_j}} \mathbf{A}^{-1/2} \mathbf{H}_{\mathbf{y}} \psi_{t'_j}^A(\mathbf{y}_0) \mathbf{A}^{-1/2}. \end{aligned} \quad (49)$$

For the Dirichlet term, we denote  $\phi_{i,t_j}^A(\eta_0)$  as the contribution of the integration over  $t_j$  to  $\phi_i^A(\eta)$ . Based on the derivations in Section 4.2, we have:

$$\phi_{i,t_j}^A(\eta_0) = \phi_{i,t'_j}(\mathbf{y}_0). \quad (50)$$

Then, the gradient  $\nabla_\eta \phi_{i,t_j}^A(\eta_0)$  and Hessian  $\mathbf{H}_\eta \phi_{i,t_j}^A(\eta_0)$  can be calculated as:

$$\begin{aligned} \nabla_\eta \phi_{i,t_j}^A(\eta_0) &= \mathbf{A}^{-1/2} \nabla_{\mathbf{y}} \phi_{i,t'_j}(\mathbf{y}_0) \\ \mathbf{H}_\eta \phi_{i,t_j}^A(\eta_0) &= \mathbf{A}^{-1/2} \mathbf{H}_{\mathbf{y}} \phi_{i,t'_j}(\mathbf{y}_0) \mathbf{A}^{-1/2}. \end{aligned} \quad (51)$$

Thus, the computation of the derivatives of the anisotropic Green coordinates is transformed into the isotropic formulation, and can be computed by the method described in Appendix B.

We now formulate the objective function for variational deformation. We express the deformation mapping  $f_{\mathbf{a},\mathbf{b}}(\eta)$  in matrix form as:

$$f_{\mathbf{a},\mathbf{b}}(\eta)_{1 \times d} = (\Phi_{1 \times n} \quad \Psi_{1 \times m}) \begin{pmatrix} \mathbf{a}_{n \times d} \\ \mathbf{b}_{m \times d} \end{pmatrix}, \quad (52)$$

where  $n = |\mathbb{V}|$  denotes the number of vertices, and  $m = |\mathbb{T}|$  represents the number of faces. The vector  $\Phi$  is a row vector composed of all Dirichlet terms  $\phi_i^A(\eta)$ , and  $\Psi$  is a row vector composed of all Neumann terms  $\psi_i^A(\eta)$ .

The Jacobian matrix  $\mathbf{J}_f(\eta)$  and the Hessian  $\mathbf{H}_f(\eta)$  of the deformation mapping  $f_{\mathbf{a},\mathbf{b}}(\eta)$  are also linear in  $\mathbf{a}$  and  $\mathbf{b}$ , and are expressed as follows:

$$(\mathbf{J}_f(\eta))_{d \times d}^\top = ((\mathbf{G}_\Phi)_{d \times n} \quad (\mathbf{G}_\Psi)_{d \times m}) \begin{pmatrix} \mathbf{a}_{n \times d} \\ \mathbf{b}_{m \times d} \end{pmatrix}, \quad (53)$$

where each column of  $\mathbf{G}_\Phi$  captures the gradients of  $\phi_i^A(\eta)$ , and each column of  $\mathbf{G}_\Psi$  records the gradients of  $\psi_i^A(\eta)$ . Moreover,

$$(\mathbf{H}_f(\eta))_{[d(d+1)/2] \times d} = \begin{pmatrix} (\mathbf{H}_\Phi)_{[d(d+1)/2] \times n} & (\mathbf{H}_\Psi)_{[d(d+1)/2] \times m} \end{pmatrix} \begin{pmatrix} \mathbf{a}_{n \times d} \\ \mathbf{b}_{m \times d} \end{pmatrix}, \quad (54)$$

where each column of  $\mathbf{H}_\Phi$  records the elements of the Hessian matrix of  $\phi_i^A(\eta)$ , comprising  $d(d+1)/2$  values. This vector is derived by flattening the symmetric Hessian matrix, retaining the diagonal elements and the upper-right components. Similarly,  $\mathbf{H}_\Psi$  contains the elements of the Hessian matrix of  $\psi_i^A(\eta)$ .

Based on the above formulation, we can now define an optimization framework. The energy functional  $E(f_{\mathbf{a},\mathbf{b}})$  is designed to enforce as-rigid-as-possible (ARAP) behavior at specific points (typically medial axis points), ensure global smoothness (by minimizing the Hessian magnitude), and satisfy user constraints at designated points (i.e., deforming specific points to the user-defined positions). For discrete sampling, this problem is formulated as:

$$\begin{aligned} \min_{\mathbf{a}, \mathbf{b}, \mathbf{R}_i} E(f_{\mathbf{a},\mathbf{b}}) &= \sum_{i=1}^d \|\mathbf{J}_f(\mathbf{m}_i) - \mathbf{R}_i\|_F^2 + \lambda_1 \sum_{i=1}^r \|f_{\mathbf{a},\mathbf{b}}(\mathbf{q}_i) - \mathbf{f}_i\|_2^2 \\ &+ \lambda_2 \sum_{i=1}^k \|\mathbf{H}_f(\mathbf{w}_i)\|_F^2 + \lambda_3 (\|\mathbf{a} - \mathbf{a}_0\|_F^2 + \|\mathbf{b} - \mathbf{b}_0\|_F^2), \\ \text{s.t.}, \mathbf{R}_i^\top \mathbf{R}_i &= \mathbf{I}, \forall i = 1, \dots, d. \end{aligned} \quad (55)$$

Here,  $\mathbf{a}_0$  and  $\mathbf{b}_0$  denote the values of the input source cage. This formulation aligns more closely with [Michel et al. 2025] than with the earlier work [Ben-Chen et al. 2009], which employs soft positional constraints  $\|f_{\mathbf{a},\mathbf{b}}(\mathbf{q}_i) - \mathbf{f}_i\|_2^2$ . Experiments demonstrate that soft constraints can effectively satisfy the requirements. Since the number of optimized variables is typically much larger than the number of constraints, we incorporate a regularization term  $\|\mathbf{a} - \mathbf{a}_0\|_F^2 + \|\mathbf{b} - \mathbf{b}_0\|_F^2$  to enhance the optimization stability. Further details regarding parameter selection and sampling point selection will be provided in the experiment section. We apply the local/global strategy to solve Eq. (55) [Ben-Chen et al. 2009; Liu et al. 2008; Sorkine and Alexa 2007]. Specifically, in the local step, we fix  $\mathbf{a}$  and  $\mathbf{b}$  to solve for the optimal rotation matrices  $\mathbf{R}_i$ . This step formulates a well-known orthogonal Procrustes problem, which can be efficiently solved via singular value decomposition. In the global step, we fix  $\mathbf{R}_i$  to solve for  $\mathbf{a}$  and  $\mathbf{b}$ , resulting in an unconstrained least-squares problem that can be directly reduced to a linear system.

## 7 Experiments

This section presents the experimental results of our proposed method. We first focus on cage-based deformation and demonstrate the results obtained with different coefficient matrices  $\mathbf{A}$ . Subsequently, we showcase variational deformation outcomes subject to the same constraints using varying  $\mathbf{A}$ . All experiments are on a standard laptop equipped with an Intel CPU running at 2.40 GHz and 16GB of RAM.

We begin by describing how to obtain diverse matrices  $\mathbf{A}$  for our experiments, focusing initially on the 2D scenario. By the spectral theorem, any symmetric positive definite matrix  $\mathbf{A}$  can be decomposed into a diagonal matrix  $\Lambda = \text{diag}(\lambda_1, \lambda_2)$  with  $\lambda_1, \lambda_2 > 0$  and

an orthogonal matrix  $P$  such that  $A = P \Lambda P^T$ . Moreover, since flipping the sign of an eigenvector leaves  $P \Lambda P^T$  unchanged, we may choose  $P \in SO(2)$ , i.e., a rotation matrix. Therefore, we parameterize  $P = \begin{pmatrix} \cos \theta & -\sin \theta \\ \sin \theta & \cos \theta \end{pmatrix}$  and denote  $A = \mathcal{A}(\theta, \lambda_1, \lambda_2)$ . Moreover, since for any  $c \in \mathbb{R}^+$ , the equation  $\nabla \cdot (A \nabla u) = 0$  is equivalent to  $\nabla \cdot (c A \nabla u) = 0$  and leads to the same deformation mapping, we can normalize one of the diagonal entries of the matrix to 1.0 in our formulation. Appendix C.1 provides some anisotropic matrices used in 2D deformation experiments together with the  $\lambda_1, \lambda_2, \theta$  values.

The construction of 3D matrices follows a similar approach. The 3D diagonal matrix  $\Lambda$  is defined by three positive parameters  $\lambda_1, \lambda_2$  and  $\lambda_3$ . The 3D rotation matrix  $P$  is parameterized by three Euler angles  $\alpha, \beta, \gamma$  and can be expressed as  $P = R_z(\alpha)R_y(\beta)R_x(\gamma)$ , where

$$R_z(\alpha) = \begin{pmatrix} \cos \alpha & -\sin \alpha & 0 \\ \sin \alpha & \cos \alpha & 0 \\ 0 & 0 & 1 \end{pmatrix}, \quad R_y(\beta) = \begin{pmatrix} \cos \beta & 0 & -\sin \beta \\ 0 & 1 & 0 \\ \sin \beta & 0 & \cos \beta \end{pmatrix},$$

$$R_x(\gamma) = \begin{pmatrix} 1 & 0 & 0 \\ 0 & \cos \gamma & -\sin \gamma \\ 0 & \sin \gamma & \cos \gamma \end{pmatrix}. \quad (56)$$

We can denote  $A = \mathcal{A}(\lambda_1, \lambda_2, \lambda_3, \alpha, \beta, \gamma)$  for the 3D scenario.

## 7.1 Cage-based Deformation

First, we present the results of cage-based deformation using anisotropic Green coordinates with various control matrices. When  $A = I$ , our results align with those of the traditional isotropic technique [Lipman et al. 2008]. The isotropic method ensures strict angle preservation in 2D, whereas anisotropy introduces some degree of shearing. However, we will demonstrate that this capability holds considerable practical value. We start with several representative examples to demonstrate the effects generated by different matrices  $A$ , highlighting the diversity of deformation styles and options offered by our method. Additionally, we demonstrate scenarios in which anisotropic deformation potentials yield superior results, characterized by enhanced visual quality, tighter adherence to the deformed cage, or reduced isotropic or area distortion. These improvements are particularly evident in inputs with a high aspect ratio. Please refer to Appendix C.2 for the formula used to compute distortion. Subsequently, we will compare our method with mean value coordinates [Floater 2003] and harmonic coordinates [Joshi et al. 2007].

We first conduct experiments on 2D images composed of cubic and circular shapes. In Fig. 4, we present the deformation results of a grid-like image. The eigenvalues of the matrix are 1.0 and 4.0, while the rotation angles are  $\pi/6$  and  $\pi/3$ . Detailed parameter settings can be found in the table of Appendix C.1. The schematic coordinate frames associated with  $\lambda_1, \lambda_2$  and  $\theta$  are also indicated in the figure. We observe that different rotation matrices lead to varying degrees of “stretching” along different directions, which intuitively demonstrates the effects of anisotropy. Fig. 5 illustrates another example involving basic shapes such as cubes and circles. The eigenvalues of the non-diagonal matrix are typically 1.0 and 2.0. While isotropic Green coordinates are angle-preserving and map infinitesimal circles to infinitesimal circles, their deformation effect

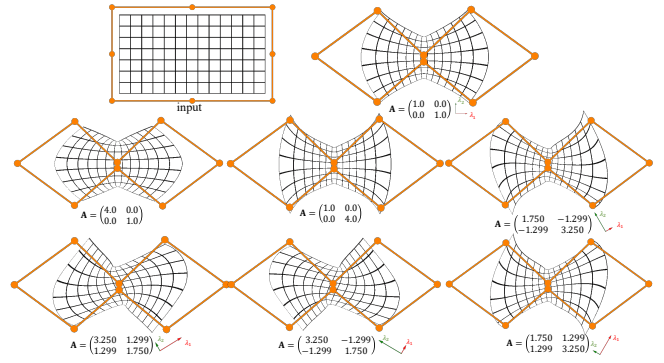


Fig. 4. Cage-based deformation of anisotropic Green coordinate in 2D. Different rotation matrices lead to varying “stretching” effects along different directions.

is fixed, which limits its flexibility and diversity. In contrast, our method enables a wide variety of deformation styles. Furthermore, regarding area distortion, the leftmost image in the middle row yields the lowest value (0.420) compared to the isotropic result (0.595).

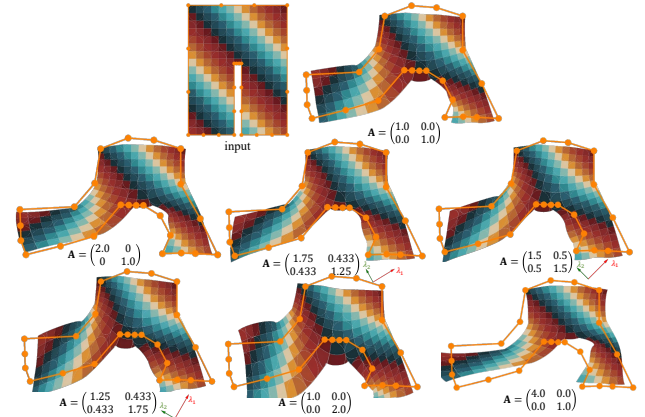


Fig. 5. Cage-based deformation results of an image containing circles and cubes. Anisotropic Green coordinates brings diverse deformation effects.

Fig. 6 shows the cage-based deformation results of a fish, an elephant, and a giraffe model, respectively. It can be observed that different matrices control the “fatness” or “thinness” of the deformed objects, thereby affording artists and animators a more versatile range of deformation choices. The crab example in Fig. 7 further demonstrates that appropriate anisotropic settings can improve deformation effects. In the figure, the tuple  $(a, b)$  represents the isometric distortion and area distortion, respectively. We can observe that the anisotropic results yield more natural deformations and exhibit lower isometric and area distortion.

To further demonstrate the advantages of our method, we compare our method with mean value coordinates (MVC) [Floater 2003] and harmonic coordinates (HC) [Joshi et al. 2007] in Fig. 8. It is

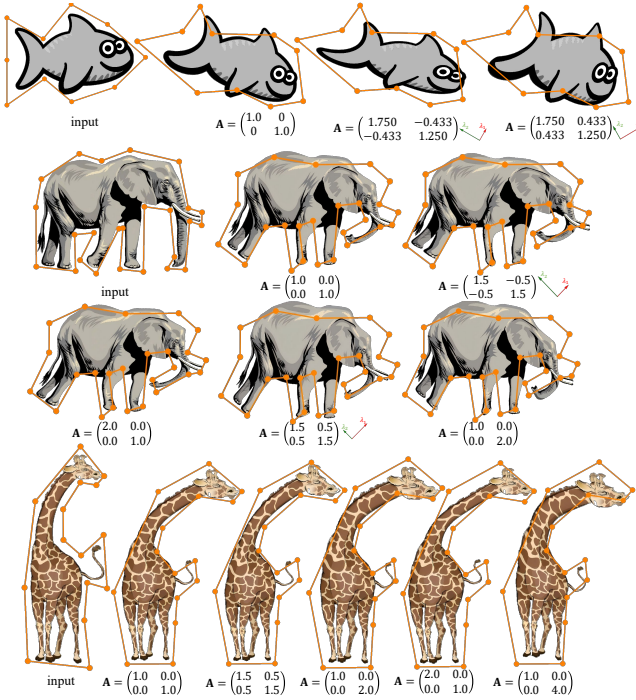


Fig. 6. Cage-based deformation results of a fish, an elephant, and a giraffe model, respectively.

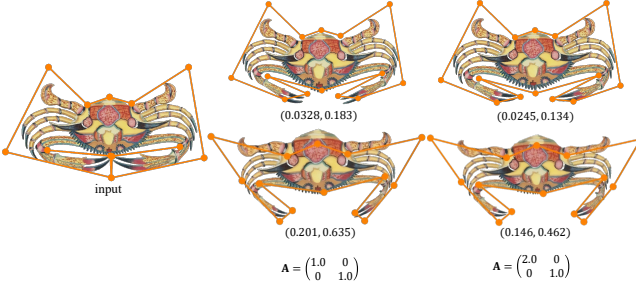


Fig. 7. Cage-based deformation results of a crab model. The tuple  $(a, b)$  represents the isometric distortion and area distortion, respectively.

evident that MVC and HC lead to noticeable shearing and unnatural deformations. Our method yields different deformation results compared to the isometric Green coordinates. Meanwhile, the quasi-conformal property of our method also guarantees a certain degree of shape preservation.

We then present the results of 3D deformation. In Fig. 9, we show the results of a bar, a bench, and a skybox model, respectively. We also mark the spatial coordinate axes in the figure. In the bar model, the deformation is mainly observed along the y-axis, while the long side is oriented along the z-axis. We show the anisotropic deformation results along the y-axis or z-axis in the coefficient matrix. It can be observed that different matrices produce deformation effects with varying degrees of sharpness. In the bench model, we observe

that different anisotropic matrices control the degree of upward bending in the chair's crossbeam. In the skybox model, the first row displays results obtained using diagonal matrices, while the second row presents outcomes for non-diagonal matrices. Specifically, from left to right, the matrices are  $A = \mathcal{A}(1.0, 0.25, 1.0, \pi/4, 0, 0)$ ,  $A = \mathcal{A}(1.0, 0.25, 1.0, \pi/4, 0, \pi/4)$  and  $A = \mathcal{A}(1.0, 0.25, 1.0, \frac{\pi}{3}, \frac{\pi}{4}, \frac{\pi}{6})$ . These experimental results further demonstrate the wide range of deformation effects achieved by our approach.

## 7.2 Variational Shape Deformation

In this subsection, we conduct experiments on variational shape deformation proposed in Section 6. Specifically, we establish the deformation mapping based on anisotropic Green coordinates as Eq. (47), and optimize  $a$  and  $b$  by enforcing spatial constraints and as-rigid-as-possible constraints, as formulated in Eq. (55). The spatial constraints dictate the deformation of  $q_i$  to  $f_i$  for  $i = 1, 2, \dots, r$ . The as-rigid-as-possible constraints aim to preserve rigidity during deformation as much as possible for some selected positions. Similar to previous methods, we sample a set of points  $m_i$  for  $i = 1, 2, \dots, d$  along the medial axis. The Hessian energy term and the regularization term ensure the smoothness of the deformation and the stability of optimization, respectively. Since harmonic functions satisfy the extremum principle at the boundary, this property is inherited by our approach, in the sense that boundary points map to boundary points under linear transformation. Consequently, we sample the boundary points  $w_i$  ( $i = 1, 2, \dots, k$ ) near the cage faces.

Figures 10 and 11 illustrate the 2D and 3D results, respectively, which are obtained using the same input and keeping all parameters constant except for the anisotropic matrix. Red dots denote the user-specified pre-deformation positions, while blue dots mark the target positions. The 2D input cages are illustrated in orange lines. The parameters are configured as  $\lambda_1 = 100$ ,  $\lambda_2 = 10$  and  $\lambda_3 = 0.1$ . In the first two examples, we sample ten boundary points near each cage face to compute the Hessians, whereas for the final example, we sample two points near each face. The results demonstrate that varying the anisotropic matrices yields different deformation outcomes, thereby expanding the range of achievable deformation effects. In the 3D scenario, we also use red and blue points to mark the points of spatial constraints. Furthermore, we manually annotate the constraints that are occluded during rendering. The initial cages are dense, subdivided rectangular triangle meshes enclosing the entire input. We sample two points near each face to compute the Hessians. The parameters are set to  $\lambda_1 = 1000$ ,  $\lambda_2 = 0.5$  and  $\lambda_3 = 0.001$  for the bar model (left), and to  $\lambda_1 = 100$ ,  $\lambda_2 = 0.05$  and  $\lambda_3 = 0.001$  for the Botijo model (right). These results further demonstrate the variety of deformation effects achieved by our method.

## 8 Conclusion

In this work, we introduce anisotropic Green coordinates, which incorporate a symmetric positive definite coefficient matrix into the divergence operator of the Laplacian equation. This approach enables a variety of deformation styles for both cage-based deformation and variational shape deformation. We derive the Green's identity based on the anisotropic Laplacian equation and demonstrate that our method satisfies both linear precision and translation

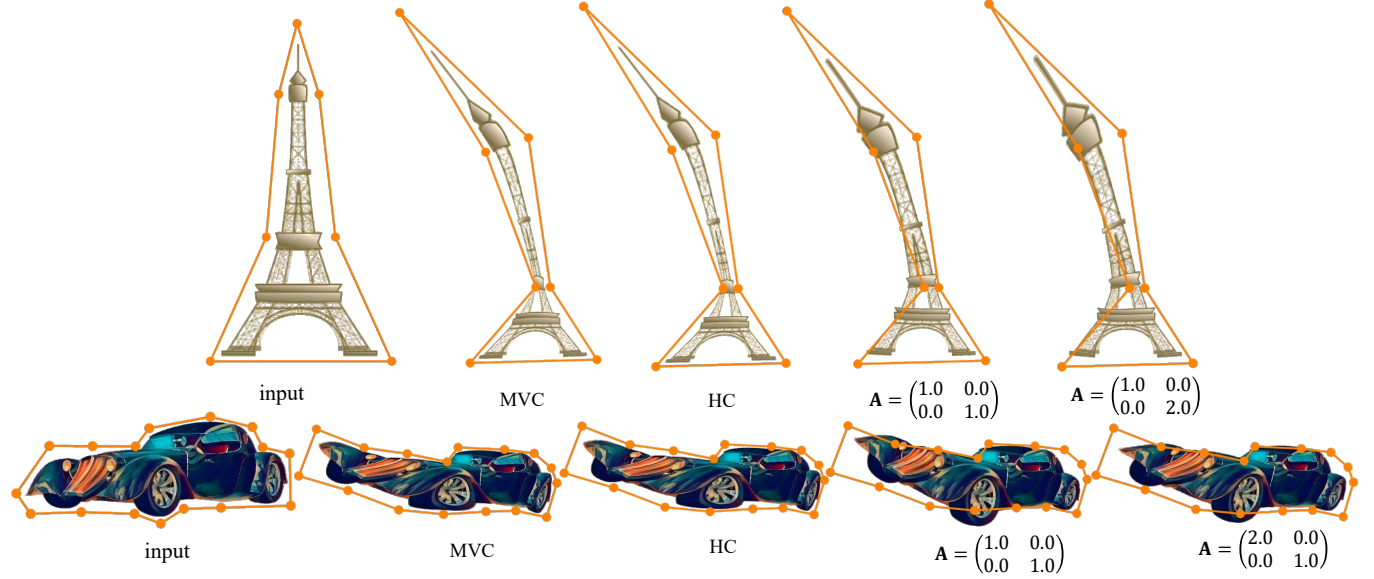


Fig. 8. Comparison of cage-based deformation results using our method, MVC [Floater 2003], and HC [Joshi et al. 2007].

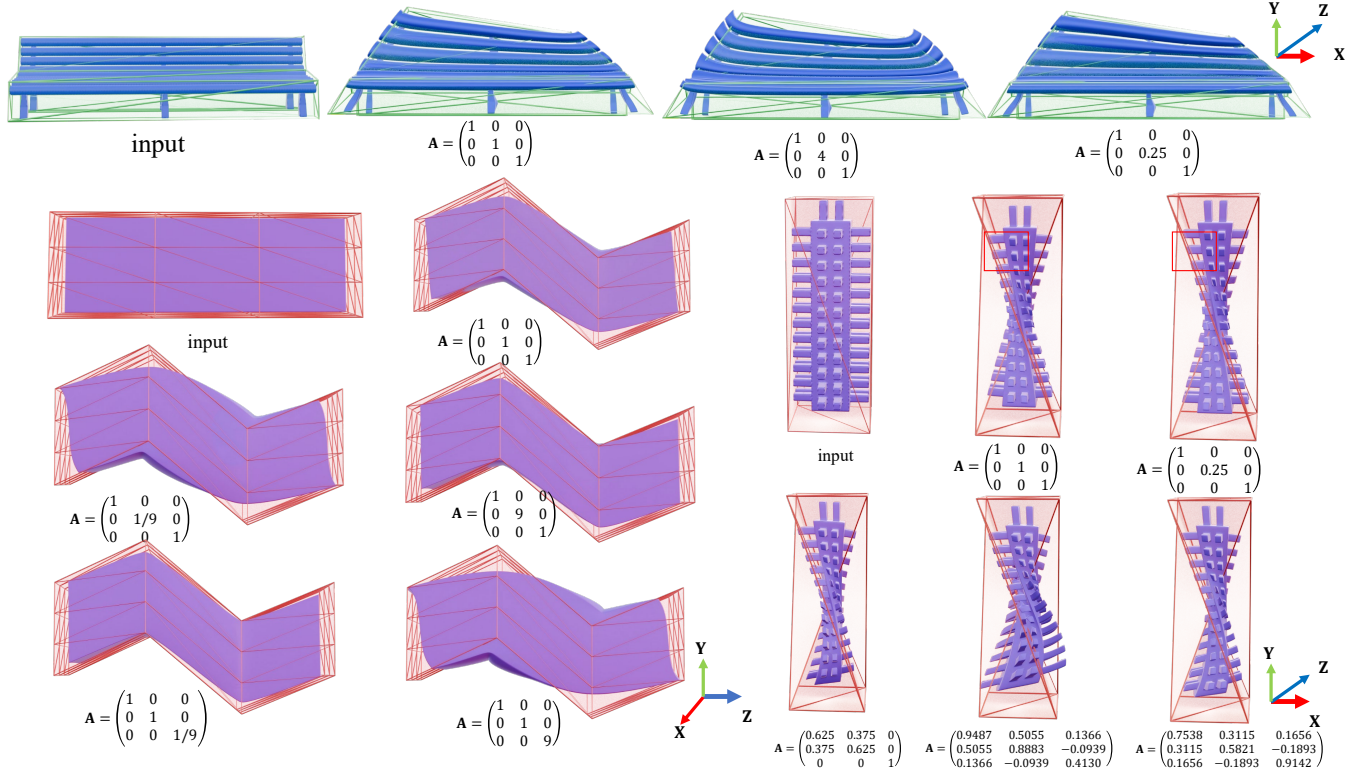


Fig. 9. Cage-based deformation results of a bar, a bench and a skybox model in 3D, respectively.

invariance. Furthermore, anisotropic Green coordinates, along with their gradients and Hessians, admit closed-form expressions. This

facilitates the efficient computation of deformation mappings and

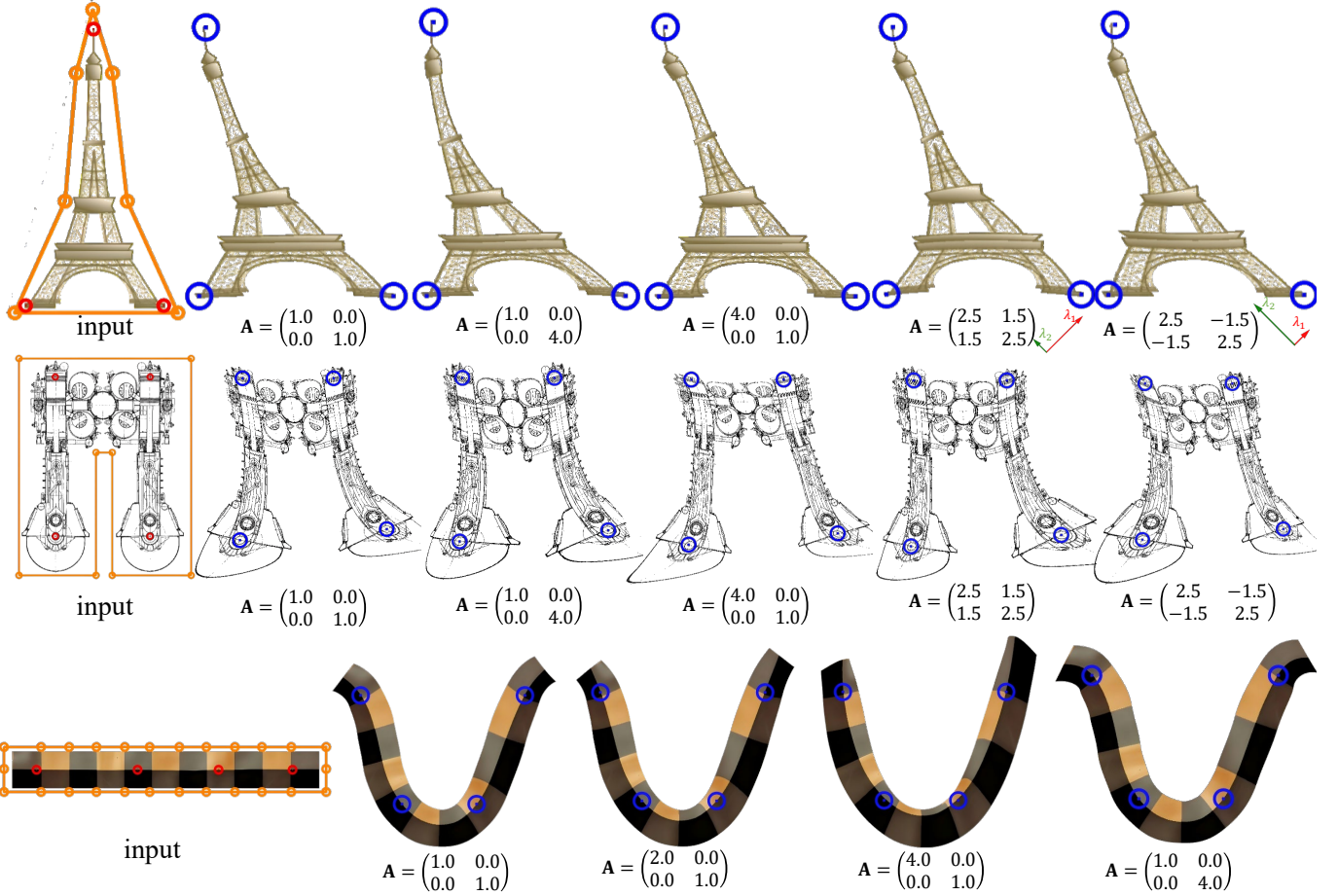


Fig. 10. Results of variational shape deformation in 2D. The red dots indicate the user-specified pre-deformation positions, while the blue dots mark the target positions.

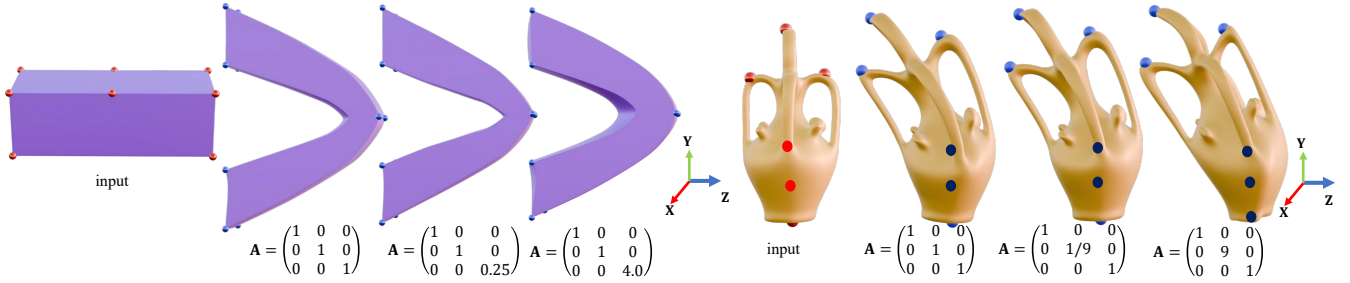


Fig. 11. Results of variational shape deformation in 3D. Red and blue dots mark the spatial constraints.

supports variational shape deformation using as-rigid-as-possible energy, while accommodating user-specified positional constraints.

The primary limitation of our method is that the matrix  $A$  remains globally invariant and is not optimized based on deformation constraints, which we leave to future work. Additionally, Green coordinates cannot satisfy both Dirichlet and Neumann boundary

conditions simultaneously. We adopt Green coordinates as the foundation of our approach because of their theoretical elegance and strong compatibility with the concept of anisotropy. We anticipate that this framework will offer novel insights for anisotropic space deformation and inspire further research in this field.

## References

Alexander G. Belyaev. 2006. On transfinite barycentric coordinates. In *Proceedings of the Fourth Eurographics Symposium on Geometry Processing (ACM International Conference Proceeding Series, Vol. 256)*. 89–99.

Mirela Ben-Chen, Ofir Weber, and Craig Gotsman. 2009. Variational harmonic maps for space deformation. *ACM Transactions on Graphics* 28, 3 (2009), 34.

Qingjun Chang, Chongyang Deng, and Kai Hormann. 2023. Maximum likelihood coordinates. *Computer Graphics Forum* 42, 5 (2023), i–viii.

Qingjun Chang and Kai Hormann. 2025. Transfinite barycentric coordinates for arbitrary planar domains. *Computer Aided Geometric Design* 119 (2025), 102433.

Jiong Chen, Fernando de Goes, and Mathieu Desbrun. 2023. Somigliana coordinates: an elasticity-derived approach for cage deformation. In *ACM SIGGRAPH 2023 Conference Proceedings*. 52:1–52:8.

Jiong Chen and Mathieu Desbrun. 2022. Go Green: General regularized Green's functions for elasticity. In *SIGGRAPH 2022 Conference Papers*. 6:1–6:8.

Tungyang Chen and Hsin-Yi Kuo. 2005. On linking n-dimensional anisotropic and isotropic Green's functions for infinite space, half-space, bimaterial, and multilayer for conduction. *International Journal of Solids and Structures* 42, 14 (2005), 4099–4114.

Fernando de Goes and Mathieu Desbrun. 2024. Stochastic computation of barycentric coordinates. *ACM Transactions on Graphics* 43, 4 (2024), 42:1–42:13.

Ana Dodik, Oded Stein, Vincent Sitzmann, and Justin Solomon. 2023. Variational barycentric coordinates. *ACM Transactions on Graphics* 42, 6 (2023), 255:1–255:16.

Christopher Dyken and Michael S. Floater. 2009. Transfinite mean value interpolation. *Computer Aided Geometric Design* 26, 1 (2009), 117–134.

Evans and C Lawrence. 1964. Partial differential equations. *Interscience Publishers* (1964).

Michael S. Floater. 2003. Mean value coordinates. *Computer Aided Geometric Design* 20, 1 (2003), 19–27.

Michael S. Floater. 2015. Generalized barycentric coordinates and applications. *Acta Numerica* 24 (2015), 161–214.

Michael S. Floater, Géza Kós, and Martin Reimers. 2005. Mean value coordinates in 3D. *Computer Aided Geometric Design* 22, 7 (2005), 623–631.

Gerald B. Folland. 1995. *Introduction to partial differential equations* (2nd ed.). Princeton University Press.

Kai Hormann and N. Sukumar. 2008. Maximum entropy coordinates for arbitrary polytopes. *Computer Graphics Forum* 27, 5 (2008), 1513–1520.

Kai Hormann and Narayan Sukumar. 2017. *Generalized barycentric coordinates in computer graphics and computational mechanics* (1st ed.). CRC Press, Boca Raton, FL.

Pushkar Joshi, Mark Meyer, Tony DeRose, Brian Green, and Tom Sanocki. 2007. Harmonic coordinates for character articulation. *ACM Transactions on Graphics* 26, 3 (2007), 71.

Tao Ju, Scott Schaefer, and Joe D. Warren. 2005. Mean value coordinates for closed triangular meshes. *ACM Transactions on Graphics* 24, 3 (2005), 561–566.

Liliya Kharevych, Patrick Mullen, Houman Owhadi, and Mathieu Desbrun. 2009. Numerical coarsening of inhomogeneous elastic materials. *ACM Transactions on Graphics* 28, 3 (2009), 51.

Theodore Kim, Fernando de Goes, and Hayley N. Iben. 2019. Anisotropic elasticity for inversion-safety and element rehabilitation. *ACM Transactions on Graphics* 38, 4 (2019), 69:1–69:15.

Xian-Ying Li and Shi-Min Hu. 2013. Poisson coordinates. *IEEE Transactions on Visualization and Computer Graphics* 19, 2 (2013), 344–352.

Xian-Ying Li, Tao Ju, and Shi-Min Hu. 2013. Cubic mean value coordinates. *ACM Transactions on Graphics* 32, 4 (2013), 126:1–126:10.

Huancheng Lin, Floyd M. Chitalu, and Taku Komura. 2024. Analytic rotation-invariant modelling of anisotropic finite elements. *ACM Transactions on Graphics* 43, 5 (2024), 157:1–157:20.

Zhehui Lin and Renjie Chen. 2024. Polynomial Cauchy coordinates for curved cages. In *SIGGRAPH Asia 2024 Conference Papers*. 67:1–67:8.

Yaron Lipman and David Levin. 2009. Derivation and analysis of Green coordinates. *Computational Methods and Function Theory* 10, 1 (2009), 167.

Yaron Lipman, David Levin, and Daniel Cohen-Or. 2008. Green coordinates. *ACM Transactions on Graphics* 27, 3 (2008), 78.

Ligang Liu, Lei Zhang, Yin Xu, Craig Gotsman, and Steven J. Gortler. 2008. A Local/global approach to mesh parameterization. *Comput. Graph. Forum* 27, 5 (2008), 1495–1504.

Shibo Liu, Tielin Dai, Ligang Liu, and Xiao-Ming Fu. 2025a. Polynomial 2D biharmonic coordinates for high-order cages. *ACM Transactions on Graphics* 44, 4 (2025), 77:1–77:10.

Shibo Liu, Ligang Liu, and Xiao-Ming Fu. 2024. Polynomial 2D Green coordinates for high-order cages. *CoRR* abs/2408.06831 (2024). arXiv:2408.06831 <https://doi.org/10.48550/arXiv.2408.06831>

Shibo Liu, Ligang Liu, and Xiao-Ming Fu. 2025b. Closed-form Cauchy coordinates and their derivatives for 2D high-order cages. *arXiv preprint* (2025). <https://arxiv.org/html/2408.06831>

Yueji Ma, Jialu Shen, Yanzun Meng, Dong Xiao, Zuqiang Shi, and Bin Wang. 2025. Anisotropic Gauss reconstruction and global orientation with octree-based acceleration. *Computer Graphics Forum* 44, 5 (2025), e70199.

Élie Michel, Alec Jacobson, Siddhartha Chaudhuri, and Jean-Marc Thiery. 2025. Variational Green and biharmonic coordinates for 2D polynomial cages. *ACM Transactions on Graphics* 44, 4 (2025), 76:1–76:20.

Élie Michel and Jean-Marc Thiery. 2023. Polynomial 2D Green coordinates for polygonal cages. In *ACM SIGGRAPH 2023 Conference Proceedings*. 23:1–23:9.

Houman Owhadi and Lei Zhang. 2007. Metric-based upscaling. *Communications on Pure and Applied Mathematics* 60, 5 (2007), 675–723.

Ulrich Pinkall and Konrad Polthier. 1993. Computing discrete minimal surfaces and their conjugates. *Experimental Mathematics* 2, 1 (1993), 15–36.

Kaikai Qin, Yunhao Zhou, Chenhao Ying, Yajuan Li, and Chongyang Deng. 2024.  $C^0$  generalized Coons patches for high-order cage-based deformation. *ACM Transactions on Graphics* 43, 6 (2024).

Yuxue Ren, Na Lei, Hang Si, and Xianfeng David Gu. 2018. A construction of anisotropic meshes based on quasi-conformal mapping. In *27th International Meshing Roundtable (Lecture Notes in Computational Science and Engineering, Vol. 127)*. 249–267.

Olga Sorkine and Marc Alexa. 2007. As-rigid-as-possible surface modeling. In *Proceedings of the Fifth Eurographics Symposium on Geometry Processing (ACM International Conference Proceeding Series, Vol. 257)*. 109–116.

Daniel Strötter, Jean-Marc Thiery, Kai Hormann, Jiong Chen, Qingjun Chang, Sebastian Besler, Johannes Mueller-Roemer, Tamy Boubekeur, André Stork, and Dieter W. Fellner. 2024. A survey on Cage-based deformation of 3D models. *Computer Graphics Forum* 43, 2 (2024), e15060.

Jean-Marc Thiery and Tamy Boubekeur. 2022. Green coordinates for triquad cages in 3D. In *SIGGRAPH Asia 2022 Conference Papers*. 38:1–38:8.

Jean-Marc Thiery, Élie Michel, and Jiong Chen. 2024. Biharmonic coordinates and their derivatives for triangular 3D cages. *ACM Transactions on Graphics* 43, 4 (2024), 138:1–138:17.

Masataka Urago. 2000. Analytical integrals of fundamental solution of three-dimensional Laplace equation and their gradients. *Transactions of the Japan Society of Mechanical Engineers Series A* 66, 642 (2000), 254–260. in Japanese.

Ofir Weber, Mirela Ben-Chen, and Craig Gotsman. 2009. Complex barycentric coordinates with applications to planar shape deformation. *Computer Graphics Forum* 28, 2 (2009), 587–597.

Ofir Weber, Roi Poranne, and Craig Gotsman. 2012. Biharmonic coordinates. *Computer Graphics Forum* 31, 8 (2012), 2409–2422.

Xiongyu Wu, Shibo Liu, and Xiao-Ming Fu. 2025. Polynomial 3D Green coordinates and their derivatives for linear cages. *Computers & Graphics* 132 (2025), 104388.

Dong Xiao and Renjie Chen. 2025. Flexible 3D Cage-based Deformation via Green Coordinates on Bézier Patches. In *SIGGRAPH Conference Papers '25*. Article 58, 10 pages.

Zhipei Yan and Scott Schaefer. 2019. A family of barycentric coordinates for co-dimension 1 manifolds with simplicial facets. *Computer Graphics Forum* 38, 5 (2019), 75–83.

Zichun Zhong, Xiaohu Guo, Wenping Wang, Bruno Lévy, Feng Sun, Yang Liu, and Weihua Mao. 2013. Particle-based anisotropic surface meshing. *ACM Transactions on Graphics* 32, 4 (2013), 99:1–99:14.

## Supplementary Material of *Anisotropic Green Coordinates*

DONG XIAO, University of Science and Technology of China, China

RENJIE CHEN\*, University of Science and Technology of China, China

BAILIN DENG, Cardiff University, UK

### A Mathematical Details of Important Lemmas

In the main text, our derivation of the anisotropic Green coordinates relies on several lemmas. This section provides detailed derivations of these lemmas. Although many of these derivations are not mathematically advanced, they are non-trivial and may not be immediately obvious within the context of this research topic. Therefore, they are included here for clarity and completeness.

LEMMA A.1. *Let  $\mathbf{x}, \mathbf{y} \in \mathbb{R}^d$ , the matrix  $\mathbf{B} \in \mathbb{R}^{d \times d}$  is an invertible matrix such that  $\mathbf{y} = \mathbf{B}\mathbf{x}$ . Then, for a  $C^2$  scalar function  $f$  and a  $C^2$  vector-valued function  $\mathbf{F}$ , we have  $\nabla_{\mathbf{x}} f = \mathbf{B}^\top \nabla_{\mathbf{y}} f$ ,  $\mathbf{H}_{\mathbf{x}}(f) = \mathbf{B}^\top \mathbf{H}_{\mathbf{y}}(f) \mathbf{B}$  and  $\nabla_{\mathbf{x}} \cdot \mathbf{F} = \nabla_{\mathbf{y}} \cdot (\mathbf{B}\mathbf{F})$ . Here,  $\nabla_{\mathbf{x}} f$  and  $\mathbf{H}_{\mathbf{x}}(f)$  denote the gradient and Hessian of  $f$  with respect to  $\mathbf{x}$ , respectively, and  $\nabla_{\mathbf{x}} \cdot \mathbf{F}$  is the divergence of  $\mathbf{F}$  with respect to  $\mathbf{x}$ .*

PROOF. Since  $\mathbf{y} = \mathbf{B}\mathbf{x}$ , we have  $y_j = \sum_{k=1}^d B_{jk}x_k$  and  $\frac{\partial y_j}{\partial x_i} = B_{ji}$ . Therefore,

$$\frac{\partial f}{\partial x_i} = \sum_{j=1}^d \frac{\partial f}{\partial y_j} \frac{\partial y_j}{\partial x_i} = \sum_{j=1}^d \frac{\partial f}{\partial y_j} B_{ji}, \quad (1)$$

which is equivalent to  $\nabla_{\mathbf{x}} f = \mathbf{B}^\top \nabla_{\mathbf{y}} f$ .

Calculate the second derivative, we have

$$\frac{\partial^2 f}{\partial x_k \partial x_i} = \frac{\partial^2 f}{\partial x_i \partial x_k} = \frac{\partial}{\partial x_i} \left( \sum_{j=1}^d \frac{\partial f}{\partial y_j} B_{jk} \right) = \sum_{j=1}^d B_{jk} \frac{\partial}{\partial x_i} \left( \frac{\partial f}{\partial y_j} \right) = \sum_{j=1}^d B_{jk} \sum_{l=1}^d \frac{\partial^2 f}{\partial y_j \partial y_l} \frac{\partial y_l}{\partial x_i} = \sum_{j,l=1}^d B_{jk} \frac{\partial^2 f}{\partial y_j \partial y_l} B_{li}. \quad (2)$$

This implies that  $\mathbf{H}_{\mathbf{x}}(f) = \mathbf{B}^\top \mathbf{H}_{\mathbf{y}}(f) \mathbf{B}$ .

Moreover, let  $\mathbf{F} = (F_1, \dots, F_d)^\top$ , we have

$$\nabla_{\mathbf{x}} \cdot \mathbf{F} = \sum_{i=1}^d \frac{\partial F_i}{\partial x_i} = \sum_{i=1}^d \sum_{j=1}^d \frac{\partial F_i}{\partial y_j} \frac{\partial y_j}{\partial x_i} = \sum_{i=1}^d \sum_{j=1}^d \frac{\partial F_i}{\partial y_j} B_{ji} = \sum_{j=1}^d \frac{\partial}{\partial y_j} \left( \sum_{i=1}^d B_{ji} F_i \right) = \nabla_{\mathbf{y}} \cdot (\mathbf{B}\mathbf{F}), \quad (3)$$

completing the proof.  $\square$

LEMMA A.2. *Let  $f \in \mathcal{D}'(\mathbb{R}^d)$  be a scalar-valued distribution and  $\mathbf{F} = (F_1, \dots, F_d)^\top \in (\mathcal{D}'(\mathbb{R}^d))^d$  be a vector-valued distribution. Consider  $f$  and  $\mathbf{F}$  as distributions in the variables  $\mathbf{x}$  and  $\mathbf{y}$  via the invertible linear change of variables  $\mathbf{y} = \mathbf{B}\mathbf{x}$ . Then,  $\nabla_{\mathbf{x}} f = \mathbf{B}^\top \nabla_{\mathbf{y}} f$  and  $\nabla_{\mathbf{x}} \cdot \mathbf{F} = \nabla_{\mathbf{y}} \cdot (\mathbf{B}\mathbf{F})$ , where  $\nabla_{\mathbf{x}} f$  denotes the gradient of  $f$  with respect to  $\mathbf{x}$ , and  $\nabla_{\mathbf{x}} \cdot \mathbf{F}$  is the divergence of  $\mathbf{F}$  with respect to  $\mathbf{x}$ . All derivatives are interpreted in the distributional sense.*

\*Corresponding author

Authors' Contact Information: Dong Xiao, xiaodong@ustc.edu.cn, School of Mathematical Sciences, University of Science and Technology of China, China; Renjie Chen, renjiec@ustc.edu.cn, School of Mathematical Sciences, University of Science and Technology of China, China; Bailin Deng, dengb3@cardiff.ac.uk, School of Computer Science and Informatics, Cardiff University, UK.

PROOF. Let  $\varphi \in C_c^\infty(\mathbb{R}_x^d)$  be an arbitrary test function, where  $C_c^\infty(\mathbb{R}_x^d)$  denotes the space of smooth functions with compact support in  $\mathbb{R}^d$ . For a distribution  $f$ , its partial derivative  $\partial_{x_i} f$  is defined by

$$\langle \partial_{x_i} f, \varphi \rangle = -\langle f, \partial_{x_i} \varphi \rangle \text{ for all } \varphi \in C_c^\infty(\mathbb{R}_x^d). \quad (4)$$

Define  $\psi(\mathbf{y}) = \varphi(\mathbf{B}^{-1}\mathbf{y}) \in C_c^\infty(\mathbb{R}_y^d)$ . According to the distribution theory [Schwartz 1966],  $\langle u, \varphi \rangle = |\det \mathbf{B}|^{-1} \langle u, \psi \rangle$  for any distribution  $u \in \mathcal{D}'(\mathbb{R}^d)$ . By Lemma A.1 and the smoothness of  $\varphi$  and  $\psi$ , we have

$$\begin{aligned} \langle \partial_{x_i} f, \varphi \rangle &= -\langle f, \partial_{x_i} \varphi \rangle = -|\det \mathbf{B}|^{-1} \langle f, (\partial_{x_i} \varphi) \circ \mathbf{B}^{-1} \rangle = -|\det \mathbf{B}|^{-1} \langle f, \partial_{x_i} \psi \rangle = -|\det \mathbf{B}|^{-1} \langle f, \sum_{j=1}^d B_{ji} \partial_{y_j} \psi \rangle \\ &= -\sum_{j=1}^d B_{ji} |\det \mathbf{B}|^{-1} \langle f, \partial_{y_j} \psi \rangle = \sum_{j=1}^d B_{ji} |\det \mathbf{B}|^{-1} \langle \partial_{y_j} f, \psi \rangle = \sum_{j=1}^d B_{ji} \langle \partial_{y_j} f, \varphi \rangle. \end{aligned} \quad (5)$$

which implies  $\partial_{x_i} f = \sum_{j=1}^d B_{ji} \partial_{y_j} f$  in  $\mathcal{D}'(\mathbb{R}^d)$  and hence  $\nabla_{\mathbf{x}} f = \mathbf{B}^\top \nabla_{\mathbf{y}} f$ .

$\nabla_{\mathbf{x}} \cdot \mathbf{F}$  is the divergence of the vector-valued distribution  $\mathbf{F} = (F_1, F_2, \dots, F_d)^\top$  if

$$\langle \nabla_{\mathbf{x}} \cdot \mathbf{F}, \varphi \rangle = -\sum_{i=1}^d \langle F_i, \partial_{x_i} \varphi \rangle \text{ for all } \varphi \in C_c^\infty(\mathbb{R}^d). \quad (6)$$

We then have

$$\begin{aligned} \langle \nabla_{\mathbf{x}} \cdot \mathbf{F}, \varphi \rangle &= -\sum_{i=1}^d \langle F_i, \partial_{x_i} \varphi \rangle = -\sum_{i=1}^d |\det \mathbf{B}|^{-1} \langle F_i, (\partial_{x_i} \varphi) \circ \mathbf{B}^{-1} \rangle = -|\det \mathbf{B}|^{-1} \sum_{i=1}^d \langle F_i, \sum_{j=1}^d B_{ji} \partial_{y_j} \psi \rangle \\ &= -|\det \mathbf{B}|^{-1} \sum_{j=1}^d \langle \sum_{i=1}^d B_{ji} F_i, \partial_{y_j} \psi \rangle = |\det \mathbf{B}|^{-1} \langle \nabla_{\mathbf{y}} \cdot (\mathbf{B}\mathbf{F}), \psi \rangle = \langle \nabla_{\mathbf{y}} \cdot (\mathbf{B}\mathbf{F}), \varphi \rangle. \end{aligned} \quad (7)$$

Therefore,  $\nabla_{\mathbf{x}} \cdot \mathbf{F} = \nabla_{\mathbf{y}} \cdot (\mathbf{B}\mathbf{F})$  in  $\mathcal{D}'(\mathbb{R}^d)$ , which completes the proof.  $\square$

LEMMA A.3. Let  $\mathbf{x} \in \mathbb{R}^d$ ,  $\mathbf{B} \in \mathbb{R}^{d \times d}$  be an invertible matrix and  $\delta(\mathbf{x})$  be the Dirac delta distribution satisfying  $\delta(\mathbf{x}) = 0$  for  $\mathbf{x} \neq \mathbf{0}$  and  $\int_{\mathbb{R}^d} \delta(\mathbf{x}) = 1$ . Then,

$$\delta(\mathbf{B}\mathbf{x}) = \frac{1}{|\det \mathbf{B}|} \delta(\mathbf{x}). \quad (8)$$

PROOF. Let  $\mathbf{y} = \mathbf{B}\mathbf{x}$ , we have  $d\mathbf{y} = |\det \mathbf{B}| d\mathbf{x}$ . Moreover, let  $\varphi \in C_c^\infty(\mathbb{R}^d)$  be an arbitrary smooth test function with compact support. Then,

$$\int_{\mathbb{R}^d} \delta(\mathbf{B}\mathbf{x}) \varphi(\mathbf{x}) d\mathbf{x} = \int_{\mathbb{R}^d} \delta(\mathbf{y}) \varphi(\mathbf{B}^{-1}\mathbf{y}) \frac{1}{|\det \mathbf{B}|} d\mathbf{y} = \frac{1}{|\det \mathbf{B}|} \varphi(\mathbf{0}) = \frac{1}{|\det \mathbf{B}|} \int_{\mathbb{R}^d} \delta(\mathbf{x}) \varphi(\mathbf{x}) d\mathbf{x}. \quad (9)$$

Therefore, for all test functions  $\varphi$ :

$$\int_{\mathbb{R}^d} \delta(\mathbf{B}\mathbf{x}) \varphi(\mathbf{x}) d\mathbf{x} = \frac{1}{|\det \mathbf{B}|} \int_{\mathbb{R}^d} \delta(\mathbf{x}) \varphi(\mathbf{x}) d\mathbf{x}. \quad (10)$$

This implies that  $\delta(\mathbf{B}\mathbf{x}) = \frac{1}{|\det \mathbf{B}|} \delta(\mathbf{x})$ .  $\square$

LEMMA A.4. Let  $\mathbf{B}$  be an invertible matrix, and let  $\mathbf{n}$  be the normal vector of  $C$ , where  $C$  is a non-degenerate 1-simplex in  $\mathbb{R}^2$  or 2-simplex in  $\mathbb{R}^3$ . If  $C$  is transformed by  $\mathbf{B}$ , i.e., all vertices  $\mathbf{v}_i$  of  $C$  are mapped to  $\mathbf{B}\mathbf{v}_i$ . Then, the normal vector with the same orientation of the transformed simplex  $C'$  is given by  $\frac{\mathbf{B}^{-\top} \mathbf{n}}{||\mathbf{B}^{-\top} \mathbf{n}||}$ .

PROOF. Let  $\mathbf{v}_1, \mathbf{v}_2 \in \mathbb{R}^2$ . By definition,  $\mathbf{n} \cdot (\mathbf{v}_2 - \mathbf{v}_1) = 0$ . Then,

$$(\mathbf{B}^{-\top} \mathbf{n}) \cdot (\mathbf{B}\mathbf{v}_2 - \mathbf{B}\mathbf{v}_1) = \mathbf{n}^\top \mathbf{B}^{-1} \mathbf{B}(\mathbf{v}_2 - \mathbf{v}_1) = \mathbf{n} \cdot (\mathbf{v}_2 - \mathbf{v}_1) = 0. \quad (11)$$

Therefore,  $\frac{\mathbf{B}^{-\top} \mathbf{n}}{\|\mathbf{B}^{-\top} \mathbf{n}\|}$  is the normal vector of  $C'$ . Moreover, if  $\mathbf{p}$  in  $\mathbb{R}^2$  satisfies  $\mathbf{n} \cdot (\mathbf{p} - \mathbf{v}_1) > 0$ , we also have  $(\mathbf{B}^{-\top} \mathbf{n}) \cdot (\mathbf{B}\mathbf{p} - \mathbf{B}\mathbf{v}_1) > 0$ , which proves the orientation consistency.

Let  $\mathbf{v}_1, \mathbf{v}_2, \mathbf{v}_3 \in \mathbb{R}^3$ . By definition,  $\mathbf{n} \cdot (\mathbf{v}_2 - \mathbf{v}_1) = 0$  and  $\mathbf{n} \cdot (\mathbf{v}_3 - \mathbf{v}_1) = 0$ . Similarly to the 2D case, we have  $(\mathbf{B}^{-\top} \mathbf{n}) \cdot (\mathbf{B}\mathbf{v}_2 - \mathbf{B}\mathbf{v}_1) = 0$  and  $(\mathbf{B}^{-\top} \mathbf{n}) \cdot (\mathbf{B}\mathbf{v}_3 - \mathbf{B}\mathbf{v}_1) = 0$ . Therefore,  $\frac{\mathbf{B}^{-\top} \mathbf{n}}{\|\mathbf{B}^{-\top} \mathbf{n}\|}$  is the normal vector of  $C'$ . Moreover, if  $\mathbf{p}$  in  $\mathbb{R}^3$  satisfies  $\mathbf{n} \cdot (\mathbf{p} - \mathbf{v}_1) > 0$ , we also have  $(\mathbf{B}^{-\top} \mathbf{n}) \cdot (\mathbf{B}\mathbf{p} - \mathbf{B}\mathbf{v}_1) > 0$ , which proves the orientation consistency.  $\square$

LEMMA A.5. *Let  $C$  be a regular curve in  $\mathbb{R}^2$  parameterized by  $\mathbf{r}(u)$  with the length element  $ds(u) = \|\mathbf{r}_u\| du$ .  $C'$  is the curve obtained by applying an invertible linear transformation  $\mathbf{B}$  to  $C$ , i.e.,  $C'$  is parameterized by  $\mathbf{s}(u) = \mathbf{B}\mathbf{r}(u)$ . Then the length element  $ds'(u)$  of  $C'$  at  $u$  is given by:*

$$ds'(u) = \|\mathbf{B}\mathbf{t}(u)\| ds(u), \quad (12)$$

where  $\mathbf{t}(u)$  is the unit tangent vector to  $C$  at  $\mathbf{r}(u)$ . In particular, if  $\mathbf{B}$  is symmetric, we also have

$$ds'(u) = |\det \mathbf{B}| \|\mathbf{B}^{-1} \mathbf{n}(u)\| ds(u), \quad (13)$$

where  $\mathbf{n}(u)$  is the unit normal vector to  $C$  at  $\mathbf{r}(u)$ .

PROOF. The tangent vector of  $C'$  is  $\mathbf{s}_u = \mathbf{B}\mathbf{r}_u$ . The length element

$$ds'(u) = \|\mathbf{s}_u\| du = \|\mathbf{B}\mathbf{r}_u\| du = \|\mathbf{B}\mathbf{t}(u)\| \|\mathbf{r}_u\| du = \|\mathbf{B}\mathbf{t}(u)\| ds(u). \quad (14)$$

where  $\mathbf{t}(u)$  is the unit tangent vector to  $C$  at  $\mathbf{r}(u)$ . This completes the proof of the first part.

Without loss of generality, we can choose an orthonormal coordinate system at  $\mathbf{r}(u)$  such that  $\mathbf{t}(u) = (1, 0)^\top$  and  $\mathbf{n}(u) = (0, 1)^\top$ . When  $\mathbf{B}$  is symmetric, it can be expressed as  $\mathbf{B} = \begin{pmatrix} a & b \\ b & c \end{pmatrix}$ . We also have  $\mathbf{B}^{-1} = \frac{1}{ac-b^2} \begin{pmatrix} c & -b \\ -b & a \end{pmatrix}$ .

Therefore,  $\|\mathbf{B}\mathbf{t}(u)\| = \sqrt{a^2 + b^2}$ . Given that  $|\det \mathbf{B}| = |ac - b^2|$ , we have

$$\|\mathbf{B}^{-1} \mathbf{n}(u)\| = \left\| \frac{1}{ac-b^2} (b, -a) \right\| = \frac{\sqrt{a^2 + b^2}}{|\det \mathbf{B}|} = \frac{\|\mathbf{B}\mathbf{t}(u)\|}{|\det \mathbf{B}|}. \quad (15)$$

This completes the proof of the second part.  $\square$

LEMMA A.6. *Let  $C$  be a regular surface in  $\mathbb{R}^3$  parameterized by  $\mathbf{r}(u, v)$  with the area element  $ds(u, v) = \|\mathbf{r}_u \times \mathbf{r}_v\| dudv$ .  $C'$  is the surface obtained by applying an invertible linear transformation  $\mathbf{B}$  to  $C$ , i.e.,  $C'$  is parameterized by  $\mathbf{s}(u, v) = \mathbf{B}\mathbf{r}(u, v)$ . Then the area element  $ds'(u, v)$  of  $C'$  at  $(u, v)$  is given by:*

$$ds'(u, v) = |\det \mathbf{B}| \|\mathbf{B}^{-\top} \mathbf{n}(u, v)\| ds(u, v), \quad (16)$$

where  $\mathbf{n}(u, v)$  is the unit normal vector to  $C$  at  $\mathbf{r}(u, v)$ .

PROOF. The tangent vectors of  $C'$  are  $\mathbf{s}_u = \mathbf{B}\mathbf{r}_u$  and  $\mathbf{s}_v = \mathbf{B}\mathbf{r}_v$ . The area element on  $C'$  is given by  $ds'(u, v) = \|\mathbf{s}_u \times \mathbf{s}_v\| dudv$ . We first show that  $(\mathbf{B}\mathbf{a}) \times (\mathbf{B}\mathbf{b}) = (\det \mathbf{B})\mathbf{B}^{-\top}(\mathbf{a} \times \mathbf{b})$  for arbitrary vectors  $\mathbf{a}$  and  $\mathbf{b}$  in  $\mathbb{R}^3$ . Consider another vector  $\mathbf{c} \in \mathbb{R}^3$  and the triple scalar product:

$$\begin{aligned} \mathbf{c} \cdot [(\mathbf{B}\mathbf{a}) \times (\mathbf{B}\mathbf{b})] &= \det(\mathbf{B}\mathbf{a}, \mathbf{B}\mathbf{b}, \mathbf{c}) = \det(\mathbf{B}) \det(\mathbf{a}, \mathbf{b}, \mathbf{B}^{-1}\mathbf{c}) \\ &= \det(\mathbf{B})(\mathbf{a} \times \mathbf{b}) \cdot (\mathbf{B}^{-1}\mathbf{c}) = \det(\mathbf{B})(\mathbf{c}^\top \mathbf{B}^{-\top}(\mathbf{a} \times \mathbf{b})) = \det(\mathbf{B})(\mathbf{B}^{-\top}(\mathbf{a} \times \mathbf{b})) \cdot \mathbf{c}. \end{aligned} \quad (17)$$

Since  $\mathbf{c}$  is also arbitrary, we conclude that

$$(\mathbf{Ba}) \times (\mathbf{Bb}) = (\det \mathbf{B}) \mathbf{B}^{-\top} (\mathbf{a} \times \mathbf{b}). \quad (18)$$

Therefore,

$$\mathbf{s}_u \times \mathbf{s}_v = (\mathbf{Br}_u) \times (\mathbf{Br}_v) = (\det \mathbf{B}) \mathbf{B}^{-\top} (\mathbf{r}_u \times \mathbf{r}_v). \quad (19)$$

Taking the norms, we obtain

$$\begin{aligned} d\mathbf{s}'(u, v) &= \|\mathbf{s}_u \times \mathbf{s}_v\| \, du \, dv = |\det \mathbf{B}| \|\mathbf{B}^{-\top} (\mathbf{r}_u \times \mathbf{r}_v)\| \, du \, dv \\ &= |\det \mathbf{B}| \|\mathbf{B}^{-\top} \mathbf{n}(u, v)\| \|\mathbf{r}_u \times \mathbf{r}_v\| \, du \, dv = |\det \mathbf{B}| \|\mathbf{B}^{-\top} \mathbf{n}(u, v)\| \, ds(u, v). \end{aligned} \quad (20)$$

The third equality holds because  $\mathbf{n}(u, v) = \frac{\mathbf{r}_u \times \mathbf{r}_v}{\|\mathbf{r}_u \times \mathbf{r}_v\|}$ . This completes the proof.  $\square$

**LEMMA A.7.** *Let  $v_0, v_1, \dots, v_k$  be affinely independent points in  $\mathbb{R}^d$  with  $d \geq k$ , forming a non-degenerate  $k$ -simplex  $C$ . Then, the barycentric coordinates of any point  $p$  in  $C$  are unique with respect to  $v_0, v_1, \dots, v_k$ .*

**PROOF.** Suppose there exist two sets of barycentric coordinates  $(\lambda_0, \lambda_1, \dots, \lambda_k)$  and  $(\mu_0, \mu_1, \dots, \mu_k)$  such that:

$$p = \sum_{i=0}^k \lambda_i v_i = \sum_{i=0}^k \mu_i v_i, \quad (21)$$

where  $\lambda_i, \mu_i \geq 0$  and  $\sum_{i=0}^k \lambda_i = \sum_{i=0}^k \mu_i = 1$ . Subtracting the two representations gives

$$\sum_{i=0}^k (\lambda_i - \mu_i) v_i = 0. \quad (22)$$

Define  $\delta_i = \lambda_i - \mu_i$ , it follows that:

$$\sum_{i=0}^k \delta_i v_i = 0 \quad \text{and} \quad \sum_{i=0}^k \delta_i = 0. \quad (23)$$

Using  $v_0$  as a reference point, we have

$$\sum_{i=0}^k \delta_i v_i = \sum_{i=0}^k \delta_i (v_i - v_0) + v_0 \sum_{i=0}^k \delta_i. \quad (24)$$

According to Eq. (23) and (24), we obtain  $\sum_{i=1}^k \delta_i (v_i - v_0) = 0$ . By the affine independence of the vertices, the vectors  $v_1 - v_0, \dots, v_k - v_0$  are linearly independent. Hence,  $\delta_i = 0$  for all  $i = 1, \dots, k$ . Since  $\sum_{i=0}^k \delta_i = 0$ , we have  $\delta_0 = 0$  as well. Therefore,  $\lambda_i = \mu_i$  for all  $i = 0, 1, \dots, k$ .  $\square$

## B Closed-Form Expressions of Isotropic Green Coordinates and Their Derivatives

In this section, we present detailed derivations of closed-form expressions for the classical isotropic Green coordinates, including their gradients and Hessians, for both 2D and 3D oriented simplicial cages. These formulations form the foundation for the development of anisotropic techniques. Although these results have appeared fragmentarily in previous literature [Ben-Chen et al. 2009; Lipman and Levin 2009; Lipman et al. 2008; Michel et al. 2025; Urago 2000], to our knowledge, a systematic derivation and summary is still lacking. In particular, many publications in this field do not provide thorough derivations for the gradient and Hessian in the 3D scenario.

Mathematically, we denote the cage (2D or 3D) as  $P = (\mathbb{V}, \mathbb{T})$ , where  $\mathbb{V}$  denote the collection of the vertices and  $\mathbb{T}$  represent the collections of the face normals. Isotropic Green coordinates reproduce arbitrary point  $\eta$  within the cage

using the cage vertices  $\{\mathbf{v}_i | i \in I_V\}$  and face normals  $\{\mathbf{n}_j | j \in I_T\}$  as follows:

$$\eta = F(\eta, P) = \sum_{i \in I_V} \phi_i(\eta) \mathbf{v}_i + \sum_{j \in I_T} \psi_j(\eta) \mathbf{n}_j, \quad \eta \in \Omega, \quad (25)$$

where

$$\phi_i(\eta) = \int_{\xi \in N\{\mathbf{v}_i\}} \Gamma_i(\xi) \frac{\partial G}{\partial \mathbf{n}}(\xi, \eta) d\sigma_\xi, \quad i \in I_V, \quad (26)$$

$$\psi_j(\eta) = - \int_{\xi \in f_j} G(\xi, \eta) d\sigma_\xi, \quad j \in I_T. \quad (27)$$

Here,  $G(\xi, \eta)$  is the fundamental solution of the Laplacian equation, and  $\Gamma_i(\xi)$  is the hat-function, which equals one at vertex  $\mathbf{v}_i$ , zero at other vertices, and varies linearly over the one-ring neighborhood of  $\mathbf{v}_i$ . Our goal is to derive closed-form expressions for  $\phi_i(\eta), \psi_j(\eta)$ , along with their gradients  $\nabla_\eta \phi_i(\eta), \nabla_\eta \psi_j(\eta)$  and Hessians  $\mathbf{H}_\eta \phi_i(\eta), \mathbf{H}_\eta \psi_j(\eta)$ . For brevity and clarity, we will omit the explicit dependence on  $\eta$  in the gradient and Hessian notations when no ambiguity arises. In the following, we primarily adopt column vector notation, meaning that row vectors will be denoted with the transpose symbol  $\top$ .

### B.1 Isotropic Green coordinates for 2D

We begin by deriving the formulation for 2D, which mainly use the methods established in [Lipman and Levin 2009] and [Michel et al. 2025]. Fig. 1 provides an illustration of a 2D cage  $P$  along with its mathematical notations. We denote

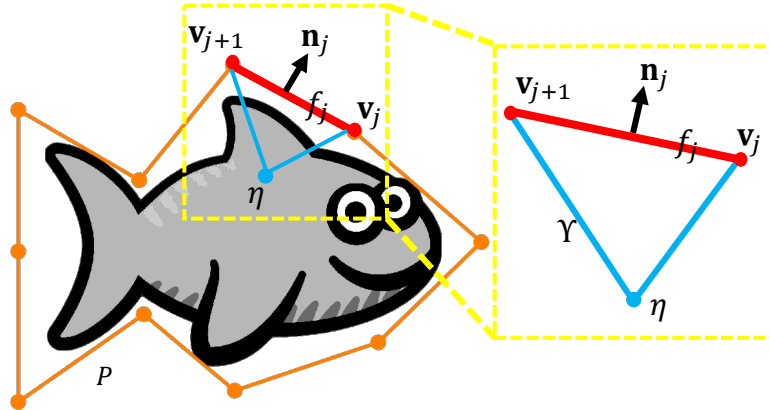


Fig. 1. Illustration of a 2D cage and its mathematical notations.

$f_j = \overrightarrow{\mathbf{v}_j \mathbf{v}_{j+1}}$  as one face of  $P$ . We first focus on computing  $\psi_j(\eta)$ , which is defined as the integral of  $-G(\xi, \eta)$  over  $f_j$ . We define  $\mathbf{a}_j = \mathbf{v}_{j+1} - \mathbf{v}_j$  and  $\mathbf{b}_j = \mathbf{v}_j - \eta$ . Consider the parametric curve  $\gamma(t) = \mathbf{v}_j + t \mathbf{a}_j$ , where  $t \in [0, 1]$ , we have:

$$\begin{aligned} \psi_j(\eta) &= - \int_{f_j} G(\xi, \eta) d\sigma_\xi = - \frac{1}{2\pi} \|\mathbf{a}_j\| \int_{t=0}^1 \log \|\mathbf{b}_j + t \mathbf{a}_j\| dt \\ &= - \frac{\|\mathbf{a}_j\|}{4\pi} \int_{t=0}^1 \log (\|\mathbf{a}_j\|^2 t^2 + 2(\mathbf{a}_j \cdot \mathbf{b}_j) t + \|\mathbf{b}_j\|^2) dt \\ &= - \frac{\|\mathbf{a}_j\|}{4\pi} (Q(1) - Q(0)), \end{aligned} \quad (28)$$

where  $Q(t)$  is the antiderivative of  $\log(\|\mathbf{a}_j\|^2 t^2 + 2(\mathbf{a}_j \cdot \mathbf{b}_j)t + \|\mathbf{b}_j\|^2)$ , which has the following expression [Lipman and Levin 2009]:

$$Q(t) = \left( t + \frac{\mathbf{a}_j \cdot \mathbf{b}_j}{\|\mathbf{a}_j\|^2} \right) \log \left( \|\mathbf{a}_j\|^2 t^2 + 2(\mathbf{a}_j \cdot \mathbf{b}_j)t + \|\mathbf{b}_j\|^2 \right) - \left( \frac{\|\mathbf{a}_j\|^2 + (\mathbf{a}_j \cdot \mathbf{b}_j)}{\|\mathbf{a}_j\|^2 \sqrt{\|\mathbf{a}_j\|^2 \|\mathbf{b}_j\|^2 - (\mathbf{a}_j \cdot \mathbf{b}_j)^2}} \right) \arctan \left( \frac{\|\mathbf{a}_j\|^2 t + (\mathbf{a}_j \cdot \mathbf{b}_j)}{\sqrt{\|\mathbf{a}_j\|^2 \|\mathbf{b}_j\|^2 - (\mathbf{a}_j \cdot \mathbf{b}_j)^2}} \right). \quad (29)$$

We now focus on the Dirichlet term  $\phi_{\mathbf{v}_j}(\eta)$ , which is defined on cage vertices  $\mathbf{v}_j$ . We denote  $\phi_{\mathbf{v}_j, f_j}(\eta)$  as the contribution of face  $f_j$  to  $\phi_{\mathbf{v}_j}(\eta)$ . The value of  $\phi_{\mathbf{v}_j}(\eta)$  is obtained by summing the contributions from all faces incident to  $\mathbf{v}_j$ . Recall that the parametric equation of  $f_j$  is  $\gamma(t) = \mathbf{v}_j + t\mathbf{a}_j$ , where  $t \in [0, 1]$ . Therefore,

$$\begin{aligned} \phi_{\mathbf{v}_j, f_j}(\eta) &= \int_0^1 (1-t) \left( \frac{\mathbf{a}_j t + \mathbf{b}_j}{2\pi \|\mathbf{a}_j t + \mathbf{b}_j\|^2} \cdot \mathbf{n}_j \right) \|\mathbf{a}_j\| dt \\ &= \frac{\|\mathbf{a}_j\| (\mathbf{b}_j \cdot \mathbf{n}_j)}{2\pi} \int_0^1 \frac{(1-t) dt}{\|\mathbf{a}_j\|^2 t^2 + 2t(\mathbf{a}_j \cdot \mathbf{b}_j) + \|\mathbf{b}_j\|^2} \\ &= -\frac{\|\mathbf{a}_j\| (\mathbf{b}_j \cdot \mathbf{n}_j)}{2\pi} (W(1) - W(0)), \end{aligned} \quad (30)$$

where  $W(t)$  is the antiderivative of  $\frac{t-1}{\|\mathbf{a}_j\|^2 t^2 + 2t(\mathbf{a}_j \cdot \mathbf{b}_j) + \|\mathbf{b}_j\|^2}$ , which is given by

$$W(t) = \frac{1}{2\|\mathbf{a}_j\|^2} \log(\|\mathbf{a}_j\|^2 t^2 + 2t(\mathbf{a}_j \cdot \mathbf{b}_j) + \|\mathbf{b}_j\|^2) - \left( \frac{\|\mathbf{a}_j\|^2 + (\mathbf{a}_j \cdot \mathbf{b}_j)}{\|\mathbf{a}_j\|^2 \sqrt{\|\mathbf{a}_j\|^2 \|\mathbf{b}_j\|^2 - (\mathbf{a}_j \cdot \mathbf{b}_j)^2}} \right) \arctan \left( \frac{\|\mathbf{a}_j\|^2 t + (\mathbf{a}_j \cdot \mathbf{b}_j)}{\sqrt{\|\mathbf{a}_j\|^2 \|\mathbf{b}_j\|^2 - (\mathbf{a}_j \cdot \mathbf{b}_j)^2}} \right). \quad (31)$$

We now proceed to compute the derivatives of  $\phi_{\mathbf{v}_j}(\eta)$  and  $\psi_j(\eta)$ . The core idea involves expressing these values in terms of integrals of rational functions with even-powered denominators with respect to the parameter  $t$ . The expressions are then subjected to partial fraction decomposition, and the integrals are evaluated using recurrence relations [Michel et al. 2025]. We denote  $\gamma_\eta(t) = \gamma(t) - \eta$ , where  $\gamma(t) = \mathbf{v}_j + t\mathbf{a}_j$ . Then we have

$$\nabla_\eta \phi_{\mathbf{v}_j, f_j}(\eta) = -\frac{\|\mathbf{a}_j\|}{2\pi} \int_{t=0}^1 (1-t) \left[ \frac{\mathbf{n}_j}{\|\gamma_\eta(t)\|^2} - 2 \frac{(\gamma_\eta(t) \cdot \mathbf{n}_j) \gamma_\eta(t)}{\|\gamma_\eta(t)\|^4} \right] dt, \quad (32)$$

$$\mathbf{H}_\eta \phi_{\mathbf{v}_j, f_j}(\eta) = -\frac{\|\mathbf{a}_j\|}{2\pi} \int_{t=0}^1 (1-t) \left[ 2 \frac{\mathbf{n}_j \gamma_\eta(t)^\top + \gamma_\eta(t) \mathbf{n}_j^\top}{\|\gamma_\eta(t)\|^4} + 2 \frac{(\gamma_\eta(t) \cdot \mathbf{n}_j) \mathbf{I}}{\|\gamma_\eta(t)\|^4} - 8 \frac{(\gamma_\eta(t) \cdot \mathbf{n}_j) \gamma_\eta(t) \gamma_\eta(t)^\top}{\|\gamma_\eta(t)\|^6} \right] dt, \quad (33)$$

$$\nabla_\eta \psi_j(\eta) = \frac{\|\mathbf{a}_j\|}{2\pi} \int_{t=0}^1 \frac{\gamma_\eta(t)}{\|\gamma_\eta(t)\|^2} dt, \quad (34)$$

$$\mathbf{H}_\eta \psi_j(\eta) = -\frac{\|\mathbf{a}_j\|}{2\pi} \int_{t=0}^1 \frac{\|\gamma_\eta(t)\|^2 \mathbf{I} - 2\gamma_\eta(t) \gamma_\eta(t)^\top}{\|\gamma_\eta(t)\|^4} dt. \quad (35)$$

Therefore, the remaining work is to compute integrals of the following form  $F_{K,n}^c = \int_0^1 \frac{t^n dt}{P_Y(t)^K}$ , where  $P_Y(t) = \|\gamma(t) - \eta\|^2$  is a polynomial of degree 2. The discriminant of  $P_Y(t) = 0$  is non-positive, and it equals zero only when the cage is concave and  $\eta$  lies on the line containing this edge. In such cases, further decomposition is unnecessary. Otherwise,  $P_Y(t) = 0$  have two complex roots satisfying  $\omega_1 = \omega_2^*$ , and  $P_Y(t)$  can be factored as

$$P_Y(t) = A(t - \omega_1)(t - \omega_2). \quad (36)$$

Then we obtain

$$F_{K,n}^c = \frac{1}{A^K} \int_0^1 \frac{t^n}{(t - \omega_1)^K (t - \omega_2)^K} dt. \quad (37)$$

We can denote  $Q = (t - \omega_1)^K(t - \omega_2)^K$ . Then,

$$\begin{aligned} \frac{1}{Q} &= \sum_{k=1}^K \frac{\alpha_k}{(t - \omega_1)^k} + \sum_{k=1}^K \frac{\beta_k}{(t - \omega_2)^k}, \text{ where} \\ \alpha_k &= \frac{1}{(K - k)!} \frac{d^{K-k}}{dt^{K-k}} \left( \frac{1}{(t - \omega_2)^K} \right) \Big|_{x=\omega_1} = (-1)^{K-k} \frac{(2K - k - 1)!}{(K - 1)!(K - k)!} (\omega_1 - \omega_2)^{-(2K-k)}, \\ \beta_k &= \frac{1}{(K - k)!} \frac{d^{K-k}}{dt^{K-k}} \left( \frac{1}{(t - \omega_1)^K} \right) \Big|_{x=\omega_2} = (-1)^{K-k} \frac{(2K - k - 1)!}{(K - 1)!(K - k)!} (\omega_2 - \omega_1)^{-(2K-k)}. \end{aligned} \quad (38)$$

The remaining terms for calculating  $F_{K,n}^c$  are all of the form  $G_{a,b}(\omega) = \int_0^1 t^a (t - \omega)^b dt$ , which can be computed using the following recursive formulation  $G_{a,b}(\omega)$ :

If  $b = -1$ , we have

$$G_{a,-1}(\omega) = \omega^a D(\omega) + U_a(\omega), \quad (39)$$

where:

$$D(\omega) = \log(1 - \omega) - \log(-\omega), \quad U_a(\omega) = \sum_{k=0}^{a-1} \frac{\omega^k}{a - k}. \quad (40)$$

If  $a = 0$ ,

$$G_{0,b}(\omega) = \frac{1}{b + 1} [(1 - \omega)^{b+1} - (-\omega)^{b+1}]. \quad (41)$$

If  $a > 0$  and  $b \neq -1$ , the recurrence relation is given by:

$$G_{a,b}(\omega) = \frac{1}{b + 1} [(1 - \omega)^{b+1} - aG_{a-1,b+1}(\omega)]. \quad (42)$$

## B.2 Isotropic Green coordinates for 3D

We now proceed to derive the isotropic Green's coordinates and their derivatives in three dimensions. This part is a central focus of this section, as to our knowledge, previous studies in the field [Ben-Chen et al. 2009], including foundational works such as [Urago 2000], have primarily provided final results while offering relatively limited elaboration on the derivation process. Consider the tetrahedron depicted in Fig. 2, which is formed by a query point  $\eta$  and a triangle  $t_j = \Delta \mathbf{v}_{j_1} \mathbf{v}_{j_2} \mathbf{v}_{j_3}$  of the 3D cage, along with other relevant mathematical notations. We compute the Neumann term  $\psi_j(\eta)$  associated with the face  $t_j$ , as well as the Dirichlet term  $\phi_{\mathbf{v}_{j_1}}(\eta)$  associate with the vertex  $\mathbf{v}_{j_1}$ , together with their gradients and Hessians. We also use  $\phi_{\mathbf{v}_{j_1}, t_j}(\eta)$  to denote the contribution of the face  $t_j$  to  $\phi_{\mathbf{v}_{j_1}}(\eta)$ . In most cases, we focus on the computation of  $\phi_{\mathbf{v}_{j_1}, t_j}(\eta)$ . However, some terms cancel out when summing over the one-ring neighbors of  $\mathbf{v}_{j_1}$  when computing  $\phi_{\mathbf{v}_{j_1}}(\eta)$ . Such instances will be explicitly indicated.

To ensure clarity in subsequent expressions, we adopt the following notation. The tetrahedron formed by  $t_j$  and  $\eta$  is denoted as  $\Upsilon$ . The outward normal of  $t_j$  is denoted as  $\mathbf{n}_t$ . Additionally, we define  $\mathbf{e}_1 = \mathbf{v}_{j_1} - \eta$ ,  $\mathbf{e}_2 = \mathbf{v}_{j_2} - \eta$ ,  $\mathbf{e}_3 = \mathbf{v}_{j_3} - \eta$ , and their corresponding unit vectors as  $\bar{\mathbf{e}}_1 = \mathbf{e}_1 / \|\mathbf{e}_1\|$ ,  $\bar{\mathbf{e}}_2 = \mathbf{e}_2 / \|\mathbf{e}_2\|$  and  $\bar{\mathbf{e}}_3 = \mathbf{e}_3 / \|\mathbf{e}_3\|$ . We also define  $R_1 = \|\mathbf{e}_2\| + \|\mathbf{e}_3\|$ ,  $R_2 = \|\mathbf{e}_3\| + \|\mathbf{e}_1\|$ ,  $R_3 = \|\mathbf{e}_1\| + \|\mathbf{e}_2\|$ ,  $\mathbf{d}_1 = \mathbf{v}_{j_2} - \mathbf{v}_{j_3}$ ,  $\mathbf{d}_2 = \mathbf{v}_{j_3} - \mathbf{v}_{j_1}$ ,  $\mathbf{d}_3 = \mathbf{v}_{j_1} - \mathbf{v}_{j_2}$ ,  $\mathbf{Z}_1 = -\mathbf{e}_2 \times \mathbf{e}_3$ ,  $\mathbf{Z}_2 = -\mathbf{e}_3 \times \mathbf{e}_1$  and  $\mathbf{Z}_3 = -\mathbf{e}_1 \times \mathbf{e}_2$ . Additionally,  $\mathbf{z}_i = \mathbf{Z}_i / \|\mathbf{Z}_i\|$  denotes the unit outward normal vector of the side faces  $S_i$  for  $i = 1, 2, 3$ . In subsequent computations, the following quantities will also be frequently used:

$$C_i = \frac{1}{4\pi \|\mathbf{d}_i\|} \log \left( \frac{R_i + \|\mathbf{d}_i\|}{R_i - \|\mathbf{d}_i\|} \right), \quad \bar{C}_i = \frac{1}{2\pi (R_i + \|\mathbf{d}_i\|)(R_i - \|\mathbf{d}_i\|)}, \quad i = 1, 2, 3, \quad (43)$$

$$P_t = \mathbf{n}_t \times \sum_{i=1}^3 C_i \mathbf{d}_i - \omega_t \mathbf{n}_t, \quad (44)$$

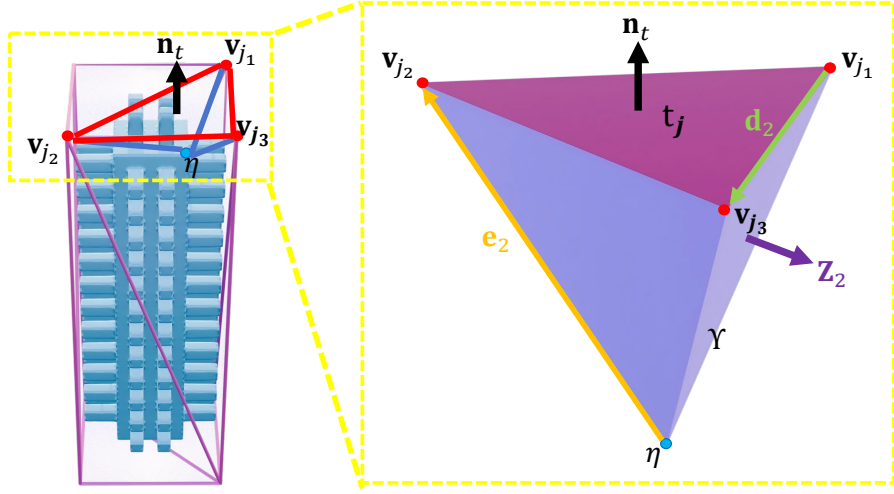


Fig. 2. Illustration of a tetrahedron formed by a query point  $\eta$  and a triangle  $t_j = \Delta v_{j_1}v_{j_2}v_{j_3}$  of the 3D cage, along with other mathematical notations for important variables.

where  $4\pi\omega_t$  is the signed solid angle of  $t_j$  toward  $\eta$ . We also define  $A_t$  as the area of  $t_j$ , and  $vol_t$  as the signed volume of  $\Upsilon$ . Moreover,  $H_t$  is the signed height of  $\eta$  to  $t_j$ . In our formulation, when  $\eta$  is in the direction opposite to  $n_j$ , as shown in Fig. 2, we define  $\omega_t$ ,  $H_t$  and  $vol_t$  as positive.

**1. Derivation of  $\psi_j(\eta)$ .** We first focus on the calculation of  $\psi_j(\eta)$ , which is the integral of  $-G(\xi, \eta)$  over  $t_j$  as

$$\psi_j(\eta) = - \int_{t_j} G(\xi, \eta) d\sigma_\xi, \quad (45)$$

we first begin with the divergence theorem of the tetrahedron  $\Upsilon$  as

$$\begin{aligned} \int_{\Upsilon} \nabla_\xi \cdot (G(\xi, \eta) n_j) dV_\xi &= \int_{t_j + S_1 + S_2 + S_3} G(\xi, \eta) (n_t \cdot n(\xi)) d\sigma_\xi \\ &= \int_{t_j} G(\xi, \eta) d\sigma_\xi + (n_t \cdot z_1) \int_{S_1} G(\xi, \eta) d\sigma_\xi + (n_t \cdot z_2) \int_{S_2} G(\xi, \eta) d\sigma_\xi + (n_t \cdot z_3) \int_{S_3} G(\xi, \eta) d\sigma_\xi. \end{aligned} \quad (46)$$

The left-hand side of the above equation can be calculated as:

$$\begin{aligned} \int_{\Upsilon} \nabla_\xi \cdot (G(\xi, \eta) n_t) dV_\xi &= \int_{\Upsilon} \nabla_\xi G(\xi, \eta) \cdot n_t dV_\xi = \int_{h=0}^{H_t} \left( \int_{S(h)} \nabla_\xi G(\xi, \eta) \cdot n_t dS \right) dh \\ &= \omega_t \int_{h=0}^{H_t} dh = \omega_t H_t = \frac{3\omega_t vol_t}{A_t}, \end{aligned} \quad (47)$$

Then we consider the integration of  $G(\xi, \eta)$  over the side face  $\Delta \eta v_{j_1} v_{j_2}$ , which is equivalent to the integration over  $\Delta \mathbf{O} v'_{j_1} v'_{j_2}$ , where  $\mathbf{O}$  is the origin,  $v'_{j_1} = v_{j_1} - \eta$  and  $v'_{j_2} = v_{j_2} - \eta$ . In Fig. 3, the region of integration is represented using polar coordinates  $R(\theta)$ . We also use  $\alpha$ ,  $\beta$  and  $\theta$  to denote key angular variables. According to the law of sines, we have

$$R(\theta) = \frac{\|\mathbf{e}_1\| \sin(\alpha)}{\sin(\pi - \alpha - \theta)}. \quad (48)$$

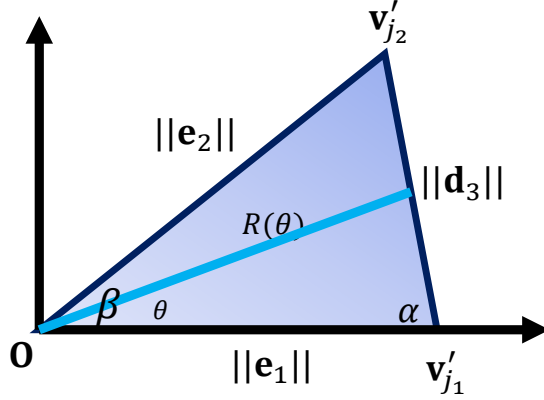


Fig. 3. Illustration of the integral of  $G(\xi, \eta)$  over the side face, along with other mathematical notations for important variables.

Then, the integral of  $G(\xi, \eta)$  over  $\Delta Ov'_{j1}v'_{j2}$  can be computed as:

$$\begin{aligned} \int_{\Delta Ov'_{j1}v'_{j2}} G(\xi, \eta) d\sigma_\xi &= -\frac{1}{4\pi} \int_{\theta=0}^{\beta} \int_{r=0}^{R(\theta)} \frac{1}{r} \times r dr d\theta = -\frac{1}{4\pi} \int_{\theta=0}^{\beta} R(\theta) d\theta = -\frac{1}{4\pi} \int_{\theta=0}^{\beta} \frac{\|e_1\| \sin(\alpha)}{\sin(\alpha + \theta)} d\theta. \\ &= -\frac{\|e_1\| \sin(\alpha)}{4\pi} \int_{\theta=\alpha}^{\alpha+\beta} \csc \theta d\theta = -\frac{\|e_1\| \sin(\alpha)}{8\pi} \log \left| \frac{1 - \cos \theta}{1 + \cos \theta} \right| \Big|_{\alpha}^{\alpha+\beta}. \end{aligned} \quad (49)$$

Additionally, we have

$$\cos(\alpha + \beta) = -\cos(\pi - \alpha - \beta) = \frac{\|e_1\|^2 - \|e_2\|^2 - \|d_3\|^2}{2\|e_2\|\|d_3\|}, \quad \cos \alpha = \frac{\|d_3\|^2 + \|e_1\|^2 - \|e_2\|^2}{2\|e_1\|\|d_3\|}. \quad (50)$$

Therefore,

$$\begin{aligned} \log \left| \frac{1 - \cos \theta}{1 + \cos \theta} \right| \Big|_{\alpha}^{\alpha+\beta} &= \log \frac{(\|e_2\| + \|d_3\|)^2 - \|e_1\|^2}{\|e_1\|^2 - (\|e_2\| - \|d_3\|)^2} - \log \frac{(\|e_1\| + \|d_3\|)^2 - \|e_2\|^2}{\|e_2\|^2 - (\|e_1\| - \|d_3\|)^2} \\ &= 2 \log \frac{\|e_1\| + \|e_2\| + \|d_3\|}{\|e_1\| + \|e_2\| - \|d_3\|}. \end{aligned} \quad (51)$$

Thus,

$$\int_{\Delta Ov'_{j1}v'_{j2}} G(\xi, \eta) d\sigma_\xi = -\frac{\|e_1\| \sin(\alpha)}{8\pi} \log \left| \frac{1 - \cos \theta}{1 + \cos \theta} \right| \Big|_{\alpha}^{\alpha+\beta} = -\frac{\|e_1 \times e_2\|}{4\pi \|d_3\|} \log \frac{\|e_1\| + \|e_2\| + \|d_3\|}{\|e_1\| + \|e_2\| - \|d_3\|}. \quad (52)$$

The integral of  $G(\xi, \eta)$  over  $\Delta Ov'_{j2}v'_{j3}$  and  $\Delta Ov'_{j3}v'_{j1}$  can be evaluated using the same approach. Then, we can obtain the closed-form formula for  $\psi_j(\eta)$  as

$$\begin{aligned} \psi_j(\eta) &= - \int_{t_j} G(\xi, \eta) d\sigma_\xi = -\frac{1}{4\pi} \left( \frac{\mathbf{e}_1 \times \mathbf{e}_2}{\|\mathbf{d}_3\|} \log \frac{\|\mathbf{e}_1\| + \|\mathbf{e}_2\| + \|\mathbf{d}_3\|}{\|\mathbf{e}_1\| + \|\mathbf{e}_2\| - \|\mathbf{d}_3\|} \right. \\ &\quad \left. + \frac{\mathbf{e}_2 \times \mathbf{e}_3}{\|\mathbf{d}_1\|} \log \frac{\|\mathbf{e}_2\| + \|\mathbf{e}_3\| + \|\mathbf{d}_1\|}{\|\mathbf{e}_2\| + \|\mathbf{e}_3\| - \|\mathbf{d}_1\|} + \frac{\mathbf{e}_3 \times \mathbf{e}_1}{\|\mathbf{d}_2\|} \log \frac{\|\mathbf{e}_3\| + \|\mathbf{e}_1\| + \|\mathbf{d}_2\|}{\|\mathbf{e}_3\| + \|\mathbf{e}_1\| - \|\mathbf{d}_2\|} \right) \cdot \mathbf{n}_t - \frac{3}{A_t} \omega_t vol_t. \end{aligned} \quad (53)$$

Therefore,

$$\boxed{\psi_t(\eta) = - \sum_{i=1}^3 C_i (\mathbf{Z}_i \cdot \mathbf{n}_t) - \frac{3}{A_t} \omega_t \text{vol}_t.} \quad (54)$$

**2. Derivation of  $\phi_{v_{j_1}}(\eta)$ .** We begin by extending the hat-function  $\Gamma_{v_{j_1}, t_j}(\xi)$  from face  $t_j$  to the entire volume of  $\Upsilon$ . Recall that  $\Gamma_{v_{j_1}, t_j}(\xi)$  takes the value 1 at  $v_{j_1}$ , 0 at its adjacent vertices, and varies linearly within the 1-neighborhood of  $v_{j_1}$ . Mathematically, for  $\xi \in \Upsilon$ ,  $\Gamma_{v_{j_1}, t_j}(\xi)$  is given by 1.0 minus the ratio of the volumes of the tetrahedron  $\xi, v_{j_2}, v_{j_3}, \eta$  and  $v_{j_1}, v_{j_2}, v_{j_3}, \eta$ . We define  $\mathbf{q}$  as the foot of the perpendicular from  $v_{j_1}$  to the plane spanned by  $v_{j_2}, v_{j_3}$  and  $\eta$ . Then,

$$\Gamma_{v_{j_1}, t_j}(\xi) = 1 - \frac{(\xi - v_{j_1}) \cdot (\mathbf{q} - v_{j_1})}{\|\mathbf{q} - v_{j_1}\|^2}. \quad (55)$$

Based on the relationships between the cross product, scalar triple product, and their geometric interpretations in terms of area and volume, the gradient of  $\Gamma_{v_{j_1}, t_j}(\xi)$  can be computed as

$$\nabla_\xi \Gamma_{v_{j_1}, t_j}(\xi) = \frac{\mathbf{v}_{j_1} - \mathbf{q}}{\|\mathbf{v}_{j_1} - \mathbf{q}\|^2} = \frac{\mathbf{e}_2 \times \mathbf{e}_3}{\|\mathbf{e}_2 \times \mathbf{e}_3\|} \cdot \frac{\|\mathbf{e}_2 \times \mathbf{e}_3\|}{|\mathbf{e}_1 \cdot (\mathbf{e}_2 \times \mathbf{e}_3)|} = \frac{\mathbf{e}_2 \times \mathbf{e}_3}{|\mathbf{e}_1 \cdot (\mathbf{e}_2 \times \mathbf{e}_3)|} = -\frac{\mathbf{Z}_1}{6 \text{vol}_t}. \quad (56)$$

According to the divergence theorem,

$$\int_{\partial\Upsilon} \Gamma_{v_{j_1}, t_j}(\xi) \frac{\partial G}{\partial \mathbf{n}}(\xi, \eta) d\sigma_\xi = \int_{\Upsilon} \nabla_\xi \cdot (\Gamma_{v_{j_1}, t_j}(\xi) \nabla_\xi G(\xi, \eta)) dV_\xi. \quad (57)$$

Recall that  $\mathbf{z}_i = \mathbf{Z}_i / \|\mathbf{Z}_i\|$  is unit normal vector for  $S_i$ . We then observe that  $\nabla_\xi G(\xi, \eta) \cdot \mathbf{z}_i = 0$  in  $S_i$  for  $i = 1, 2, 3$ . Therefore, computing  $\phi_{v_{j_1}, t_j}(\eta)$  is equivalent to evaluating the right-hand side of Eq. (57). Moreover,

$$\nabla_\xi \cdot (\Gamma_{v_{j_1}, t_j}(\xi) \nabla_\xi G(\xi, \eta)) = \Gamma_{v_{j_1}, t_j}(\xi) \Delta_\xi G(\xi, \eta) + \nabla_\xi \Gamma_{v_{j_1}, t_j}(\xi) \cdot \nabla_\xi G(\xi, \eta). \quad (58)$$

Since  $\nabla_\xi G(\xi, \eta) = \delta(\xi - \eta)$ , the integration of the first term in the equation above yields only  $\Gamma_{v_{j_1}, t_j}(\eta)$ , which is vanish at  $\eta$ . Thus, we only need to compute

$$\int_{\Upsilon} \nabla_\xi G(\xi, \eta) \nabla_\xi \Gamma_{v_{j_1}, t_j}(\xi) dV_\xi = -\frac{\mathbf{Z}_1}{6 \text{vol}_t} \cdot \int_{\Upsilon} \nabla_\xi G(\xi, \eta) dV_\xi. \quad (59)$$

According to the component-wise application of the divergence theorem, we have

$$\int_{\Upsilon} \nabla_\xi G(\xi, \eta) dV_\xi = \int_{\partial\Upsilon} G(\xi, \eta) \mathbf{n}(\xi) d\sigma_\xi = \mathbf{n}_t \int_{t_j} G(\xi, \eta) d\sigma_\xi + \mathbf{z}_1 \int_{S_1} G(\xi, \eta) d\sigma_\xi + \mathbf{z}_2 \int_{S_2} G(\xi, \eta) d\sigma_\xi + \mathbf{z}_3 \int_{S_3} G(\xi, \eta) d\sigma_\xi. \quad (60)$$

According to previous calculations,  $\mathbf{z}_i \int_{S_i} G(\xi, \eta) d\sigma_\xi = -C_i \mathbf{Z}_i$  for  $i = 1, 2, 3$  (Eq (52)). If we denote  $\mathbf{L} = \int_{\Upsilon} \nabla G(\xi, \eta) dV_\xi$ , we have

$$\mathbf{L} = -\psi_t(\eta) \mathbf{n}_t - \sum_{i=1}^3 C_i \mathbf{Z}_i. \quad (61)$$

Taking the dot product with  $\mathbf{Z}_1$  gives

$$\begin{aligned} \mathbf{Z}_1 \cdot \mathbf{L} &= - \left( - \sum_{i=1}^3 C_i (\mathbf{Z}_i \cdot \mathbf{n}_t) - \frac{3}{A_t} \omega_t \text{vol}_t \right) (\mathbf{Z}_1 \cdot \mathbf{n}_t) - \sum_{i=1}^3 C_i (\mathbf{Z}_1 \cdot \mathbf{Z}_i) \\ &= - \sum_{i=1}^3 C_i (\mathbf{Z}_1 \cdot \mathbf{Z}_i - (\mathbf{Z}_1 \cdot \mathbf{n}_t)(\mathbf{Z}_i \cdot \mathbf{n}_t)) + \frac{3}{A_t} \omega_t \text{vol}_t (\mathbf{Z}_1 \cdot \mathbf{n}_t). \end{aligned} \quad (62)$$

We will now establish the coordinate system to prove the following important equation:

$$\mathbf{Z}_i - (\mathbf{Z}_i \cdot \mathbf{n}_t) \mathbf{n}_t = H_t (\mathbf{n}_t \times \mathbf{d}_i), \quad i = 1, 2, 3, \quad (63)$$

where  $H_t = \frac{3 \text{vol}_t}{A_t}$  is the height from  $\eta$  to  $t_j$ . We place  $t_j$  in the plane  $z = 0$  with outward unit normal  $\mathbf{n}_t = (0, 0, 1)$ . Then, we denote  $\mathbf{v}_{j_i} = (x_i, y_i, 0)$  for  $k = 1, 2, 3$ . We also locate  $\eta$  on  $z$ -axis and denote  $\eta = (0, 0, -H_t)$ . Then,  $\mathbf{e}_i = \mathbf{v}_{j_i} - \eta = (x_i, y_i, H_t)$ ,  $\mathbf{d}_i = \mathbf{v}_{j_{i+1}} - \mathbf{v}_{j_{i+2}} = (x_{i+1} - x_{i+2}, y_{i+1} - y_{i+2}, 0)$ . Note that indices greater than 3 should be taken modulo 3. Let  $a = x_{i+1} - x_{i+2}, b = y_{i+1} - y_{i+2}$ , we have

$$\mathbf{Z}_i = -\mathbf{e}_{i+1} \times \mathbf{e}_{i+2} = -\mathbf{e}_{i+1} \times (\mathbf{e}_{i+1} - \mathbf{d}_i) = \mathbf{e}_{i+1} \times \mathbf{d}_i = (-H_t b, H_t a, x_{i+1} b - y_{i+1} a). \quad (64)$$

Therefore, we have  $\mathbf{Z}_i - (\mathbf{Z}_i \cdot \mathbf{n}_t) \mathbf{n}_t = (-H_t b, H_t a, 0)$ . On the other hand,

$$H_t (\mathbf{n}_t \times \mathbf{d}_i) = H_t \cdot ((0, 0, 1) \times (a, b, 0)) = (-H_t b, -H_t a, 0). \quad (65)$$

We complete the proof of the equation  $\mathbf{Z}_i - (\mathbf{Z}_i \cdot \mathbf{n}_t) \mathbf{n}_t = H_t (\mathbf{n}_t \times \mathbf{d}_i)$ . Then, we have

$$\begin{aligned} \mathbf{Z}_1 \cdot \mathbf{L} &= - \sum_{i=1}^3 C_i \left( \mathbf{Z}_1 \cdot \mathbf{Z}_i - (\mathbf{Z}_1 \cdot \mathbf{n}_t) (\mathbf{Z}_i \cdot \mathbf{n}_t) \right) + \frac{3}{A_t} \omega_t \text{vol}_t (\mathbf{Z}_1 \cdot \mathbf{n}_t) \\ &= - \sum_{i=1}^3 C_i \left( \mathbf{Z}_1 \cdot (\mathbf{Z}_i - (\mathbf{Z}_i \cdot \mathbf{n}_t) \mathbf{n}_t) \right) + \frac{3}{A_t} \omega_t \text{vol}_t (\mathbf{Z}_1 \cdot \mathbf{n}_t) \\ &= - \sum_{i=1}^3 C_i \left( \mathbf{Z}_1 \cdot H_t (\mathbf{n}_t \times \mathbf{d}_i) \right) + \frac{3}{A_t} \omega_t \text{vol}_t (\mathbf{Z}_1 \cdot \mathbf{n}_t) \\ &= - \frac{3 \text{vol}_t}{A_t} \left( \mathbf{n}_t \times \sum_{i=1}^3 C_i \mathbf{d}_i - \omega_t \mathbf{n}_t \right) \cdot \mathbf{Z}_1. \end{aligned} \quad (66)$$

Recall the definition  $P_t = \mathbf{n}_t \times \sum_{i=1}^3 C_i \mathbf{d}_i - \omega_t \mathbf{n}_t$ , we get

$$\phi_{\mathbf{v}_{j_1}, t_j}(\eta) = -\frac{1}{6 \text{vol}_t} \mathbf{Z}_1 \cdot \mathbf{L} = \frac{1}{2A_t} P_t \cdot \mathbf{Z}_1. \quad (67)$$

Therefore,  $\phi_{\mathbf{v}_{j_1}}(\eta)$  is obtained by summing over the 1-ring neighbors of  $\phi_{\mathbf{v}_{j_1}, t_j}(\eta)$  as follows:

$$\phi_{\mathbf{v}_{j_1}}(\eta) = \sum_{t \in \mathcal{N}(\mathbf{v}_{j_1})} \frac{1}{2A_t} P_t \cdot \mathbf{Z}_{1,t}. \quad (68)$$

**3. Derivation of  $\nabla \psi_t(\eta)$ .** We now show that  $\mathbf{a} \cdot \nabla \psi_t(\eta) = -\mathbf{a} \cdot P_t$  for arbitrary vector  $\mathbf{a} \in \mathbb{R}^3$ . We first notice that  $\nabla_\eta G(\xi, \eta) = -\nabla_\xi G(\xi, \eta)$ . Therefore,

$$\mathbf{a} \cdot \nabla_\eta \psi_t(\eta) = -\mathbf{a} \cdot \int_{t_j} \nabla_\eta G(\xi, \eta) \, d\sigma_\xi = \int_{t_j} \mathbf{a} \cdot \nabla_\xi G(\xi, \eta) \, d\sigma_\xi. \quad (69)$$

The vector  $\mathbf{a}$  can be decomposed into tangential parts  $\mathbf{a}_{\parallel}$  and normal parts  $\mathbf{a}_{\perp}$  with respect to  $t_j$  as  $\mathbf{a}_{\perp} = (\mathbf{a} \cdot \mathbf{n}_t) \mathbf{n}_t$  and  $\mathbf{a}_{\parallel} = \mathbf{a} - \mathbf{a}_{\perp}$ . We define a tangential vector field  $\mathbf{F}(\xi)$  with respect to  $\xi$  at  $t_j$  as:

$$\mathbf{F}(\xi) = G(\xi, \eta) \mathbf{a}_{\parallel}. \quad (70)$$

Moreover, let  $\nabla_t \cdot$  be the planar divergence operator on  $t_j$ , we have  $\nabla_t \cdot \mathbf{F} = \nabla_t \cdot (G \mathbf{a}_{\parallel}) = \mathbf{a}_{\parallel} \cdot \nabla_t G$ . Since  $\nabla_t G$  is the tangential projection of  $\nabla_{\xi} G$ , we also have  $\mathbf{a}_{\parallel} \cdot \nabla_t G = \mathbf{a}_{\parallel} \cdot \nabla_{\xi} G$  on  $t_j$ . Therefore,

$$\int_{t_j} \mathbf{a}_{\parallel} \cdot \nabla_{\xi} G \, d\sigma = \int_{t_j} \nabla_t \cdot (G \mathbf{a}_{\parallel}) \, d\sigma = \int_{\partial t_j} G(\xi, \eta) (\mathbf{a}_{\parallel} \cdot \mathbf{v}) \, ds, \quad (71)$$

where  $\mathbf{v}$  is the outward unit normal along  $\partial t_j$  lying in the plane of  $t_j$ , and  $ds$  is the arc-length measure. Then,  $\mathbf{v}_i = \mathbf{n}_t \times \frac{\mathbf{d}_i}{\|\mathbf{d}_i\|}$  for  $i = 1, 2, 3$ , and

$$\mathbf{a}_{\parallel} \cdot \mathbf{v}_i = \mathbf{a} \cdot \left( \mathbf{n}_t \times \frac{\mathbf{d}_i}{\|\mathbf{d}_i\|} \right) = (\mathbf{a} \times \mathbf{n}_t) \cdot \frac{\mathbf{d}_i}{\|\mathbf{d}_i\|}. \quad (72)$$

Eq. (71) yields

$$\int_{t_j} \mathbf{a}_{\parallel} \cdot \nabla_{\xi} G \, d\sigma = \sum_{i=1}^3 \int_{\mathbf{d}_i} G(\xi, \eta) (\mathbf{a}_{\parallel} \cdot \mathbf{v}_i) \, ds = (\mathbf{a} \times \mathbf{n}_t) \cdot \sum_{i=1}^3 \frac{\mathbf{d}_i}{\|\mathbf{d}_i\|} \int_{\mathbf{d}_i} G(\xi, \eta) \, ds. \quad (73)$$

The next step is to compute the line integral of the fundamental solution  $\int_{\mathbf{d}_i} G(\xi, \eta) \, ds$ . Let  $r_k = \|\mathbf{e}_k\| = \|\mathbf{v}_{j_k} - \eta\|$  for  $k = 1, 2, 3$ . Let  $\mathbf{a} = \mathbf{e}_3$ ,  $\mathbf{b} = \mathbf{e}_2 - \mathbf{e}_3 = \mathbf{d}_1$  and define  $\gamma(t) = \mathbf{a} + t\mathbf{b}$  with  $t \in [0, 1]$ . We also have  $ds = \|\mathbf{b}\| dt$ . Therefore,

$$\int_{\mathbf{d}_1} G(\xi, \eta) \, ds = -\frac{\|\mathbf{b}\|}{4\pi} \int_0^1 \frac{dt}{\|\mathbf{a} + t\mathbf{b}\|}. \quad (74)$$

When  $A > 0$ , the following important integral formula holds:

$$\int \frac{dt}{\sqrt{At^2 + Bt + C}} = \frac{1}{\sqrt{A}} \log |2At + B + 2\sqrt{A}\sqrt{At^2 + Bt + C}| + \text{constant}, \quad (75)$$

where  $A = \|\mathbf{b}\|^2 = \|\mathbf{d}_1\|^2$ ,  $B = 2(\mathbf{a} \cdot \mathbf{b}) = 2(\mathbf{e}_2 \cdot \mathbf{d}_1) = \|\mathbf{e}_2\|^2 - \|\mathbf{e}_3\|^2 - \|\mathbf{d}_1\|^2$ ,  $C = \|\mathbf{e}_3\|^2$ . Then we have

$$\begin{aligned} \int_{\mathbf{d}_1} G(\xi, \eta) \, ds &= -\frac{1}{4\pi} \log \frac{2\|\mathbf{d}_1\|\|\mathbf{e}_2\| + 2\|\mathbf{d}_1\|^2 + (\|\mathbf{e}_2\|^2 - \|\mathbf{e}_3\|^2 - \|\mathbf{d}_1\|^2)}{2\|\mathbf{d}_1\|\|\mathbf{e}_3\| + (\|\mathbf{e}_2\|^2 - \|\mathbf{e}_3\|^2 - \|\mathbf{d}_1\|^2)} \\ &= -\frac{1}{4\pi} \log \frac{(\|\mathbf{e}_2\| + \|\mathbf{d}_1\|)^2 - \|\mathbf{e}_3\|^2}{\|\mathbf{e}_2\|^2 - (\|\mathbf{e}_3\| - \|\mathbf{d}_1\|)^2} \\ &= -\frac{1}{4\pi} \log \frac{\|\mathbf{e}_2\| + \|\mathbf{e}_3\| + \|\mathbf{d}_1\|}{\|\mathbf{e}_2\| + \|\mathbf{e}_3\| - \|\mathbf{d}_1\|}. \end{aligned} \quad (76)$$

Recall  $R_1 = \|\mathbf{e}_2\| + \|\mathbf{e}_3\| > \|\mathbf{d}_1\|$ , we have

$$\int_{\mathbf{d}_1} G(\xi, \eta) \, ds = -\frac{1}{4\pi} \log \frac{R_1 + \|\mathbf{d}_1\|}{R_1 - \|\mathbf{d}_1\|}, \quad (77)$$

which is actually  $-\|\mathbf{d}_1\|C_1$  of Eq. (43). Moreover, we have

$$\int_{t_j} \mathbf{n}_t \cdot \nabla_{\xi} G(\xi, \eta) \, d\sigma_{\xi} = \omega_t. \quad (78)$$

Recall Eqs. (73) and (78), we obtain

$$\mathbf{a} \cdot \nabla \psi_t(\eta) = (\mathbf{a}_{\parallel} + (\mathbf{a} \cdot \mathbf{n}_t)\mathbf{n}_t) \cdot \int_{t_j} \nabla_{\xi} G(\xi, \eta) \, d\sigma_{\xi} = -(\mathbf{a} \times \mathbf{n}_t) \cdot \sum_{i=1}^3 C_i \mathbf{d}_i + (\mathbf{a} \cdot \mathbf{n}_t) \omega_t. \quad (79)$$

Using the property that  $(\mathbf{a} \times \mathbf{n}_t) \cdot \mathbf{b} = \mathbf{a} \cdot (\mathbf{n}_t \times \mathbf{b})$ , we obtain

$$\mathbf{a} \cdot \nabla \psi_t(\eta) = -\mathbf{a} \cdot \left( \mathbf{n}_t \times \sum_{i=1}^3 C_i \mathbf{d}_i - \omega_t \mathbf{n}_t \right) = \mathbf{a} \cdot (-P_t). \quad (80)$$

Since  $\mathbf{a}$  is arbitrary in  $\mathbb{R}^3$ , we have

$$\boxed{\nabla \psi_t(\eta) = -P_t.} \quad (81)$$

**4. Derivation of  $\nabla \phi_{v_{j_1}}(\eta)$ .** The gradient of  $\phi_{v_{j_1},t_j}(\eta)$  with respect to  $\eta$  can be directly obtained by differentiation as

$$\nabla \phi_{v_{j_1},t_j}(\eta) = \frac{1}{2A_t} (\mathbf{J}(\mathbf{Z}_1)^\top P_t + \mathbf{J}(P_t)^\top \mathbf{Z}_1). \quad (82)$$

We first compute the Jacobian matrix of  $\mathbf{Z}_1 = -\mathbf{e}_2 \times \mathbf{e}_3$ . Consider a perturbation  $\delta\eta$  to  $\eta$ . The corresponding variations in  $\mathbf{e}_2$  and  $\mathbf{e}_3$  are  $\delta\mathbf{e}_2 = -\delta\eta$  and  $\delta\mathbf{e}_3 = -\delta\eta$ . The variation of  $\mathbf{Z}_1$  is given by:

$$\delta\mathbf{Z}_1 = -\delta(\mathbf{e}_2 \times \mathbf{e}_3) = -(\delta\mathbf{e}_2) \times \mathbf{e}_3 - \mathbf{e}_2 \times (\delta\mathbf{e}_3) = (\delta\eta) \times \mathbf{e}_3 + \mathbf{e}_2 \times (\delta\eta) = (\mathbf{e}_2 - \mathbf{e}_3) \times \delta\eta. \quad (83)$$

Hence, the Jacobian matrix of  $\mathbf{Z}_1$  is

$$\mathbf{J}(\mathbf{Z}_1) = [\mathbf{e}_2]_\times - [\mathbf{e}_3]_\times = [\mathbf{d}_1]_\times, \quad (84)$$

where  $[\mathbf{u}]_\times$  denotes the skew-symmetric matrix such that, for any vector  $\mathbf{v}$ ,  $[\mathbf{u}]_\times \mathbf{v} = \mathbf{u} \times \mathbf{v}$ . An important property that will be utilized later is that  $[\mathbf{u}]_\times^\top = -[\mathbf{u}]_\times$ .

Another important observation is that the term  $\mathbf{J}(P_t)^\top \mathbf{Z}_1$  vanishes when summed over the 1-ring neighborhood of  $\mathbf{v}_{j_1}$ . To see this, we first note that

$$\begin{aligned} \mathbf{J}(P_t)^\top \mathbf{Z}_1 &= \nabla_\eta \nabla_\eta^\top (-\psi_t(\eta)) = \nabla_\eta \left( \int_t \nabla_\xi^\top G(\xi, \eta) \, d\sigma_\xi \right) \mathbf{Z}_1 = \left( - \int_t \nabla_\xi \nabla_\xi^\top G(\xi, \eta) \, d\sigma_\xi \right) \mathbf{Z}_1 \\ &= - \int_{t_j} \nabla_\xi (\mathbf{Z}_1 \cdot (\nabla_\xi G(\xi, \eta))) \, d\sigma_\xi = - \int_{\partial t_j} (\mathbf{Z}(\xi) \cdot \nabla_\xi G(\xi, \eta)) \nu(\xi) \, ds_\xi, \end{aligned} \quad (85)$$

where  $\partial t_j$  is the boundary of  $t_j$ , and  $\nu(\xi)$  is the outward unit normal of  $\partial t_j$ .

Let  $\Omega = \bigcup_{t \in \mathcal{N}(\mathbf{v}_{j_1})} t$  denote the patch formed by the union of the triangles in the 1-ring neighborhood of  $\mathbf{v}_{j_1}$ . Upon summing over all the 1-ring neighborhoods, each interior edge contributes once positively and once negatively, canceling out to zero. The only remaining term is the boundary integral over  $\partial\Omega$  as

$$- \int_{\partial\Omega} (\mathbf{Z}(\xi) \cdot \nabla_\xi G(\xi, \eta)) \nu(\xi) \, ds_\xi. \quad (86)$$

As illustrated in Fig. 2,  $\xi - \eta$  is perpendicular to  $\mathbf{Z}_1$  when  $\xi$  lies on the edge connecting  $\mathbf{v}_{j_2}$  and  $\mathbf{v}_{j_3}$ . Therefore,  $\xi - \eta$  is perpendicular to  $\mathbf{Z}(\xi)$  on  $\partial\Omega$  and the above boundary integral equals 0. Specifically,

$$\sum_{t \in \mathcal{N}(\mathbf{v}_{j_1})} \mathbf{J}(P_t)^\top \mathbf{Z}_{1,t} = 0, \quad (87)$$

and we conclude that

$$\boxed{\nabla \phi_{v_{j_1}}(\eta) = - \sum_{t \in \mathcal{N}(\mathbf{v}_{j_1})} \frac{1}{2A_t} ([\mathbf{d}_1]_\times P_t).} \quad (88)$$

**5. Derivation of  $\mathbf{H}\psi_t(\eta)$ .** The Hessian of  $\psi_t(\eta)$  can be obtained by

$$\boxed{\mathbf{H}\psi_t(\eta) = -\mathbf{J}(P_t),} \quad (89)$$

where

$$\mathbf{J}(P_t) = \sum_{i=1}^3 (\mathbf{n}_t \times \mathbf{d}_i) \nabla C_i^\top - \mathbf{n}_t \nabla \omega_t^\top. \quad (90)$$

We also have

$$\nabla C_i = \bar{C}_i (\bar{\mathbf{e}}_{i+1} + \bar{\mathbf{e}}_{i+2}). \quad (91)$$

Therefore,

$$\boxed{\mathbf{J}(P_t) = [\mathbf{n}_t] \times (\mathbf{d}_1, \mathbf{d}_2, \mathbf{d}_3)_{3 \times 3} \begin{pmatrix} \bar{C}_1 (\bar{\mathbf{e}}_2 + \bar{\mathbf{e}}_3)^\top \\ \bar{C}_2 (\bar{\mathbf{e}}_3 + \bar{\mathbf{e}}_1)^\top \\ \bar{C}_3 (\bar{\mathbf{e}}_1 + \bar{\mathbf{e}}_2)^\top \end{pmatrix}_{3 \times 3} - \mathbf{n}_t \nabla \omega_t^\top.} \quad (92)$$

To compute the derivative of  $\omega_t$  with respect to  $\eta$ , we first calculate  $\psi_t(\eta)$ . Recall that

$$\psi_t(\eta) = - \sum_{i=1}^3 C_i (\mathbf{Z}_i \cdot \mathbf{n}_t) - \frac{3}{A_t} \omega_t \text{vol}_t, \quad (93)$$

and notice that its gradient with respect to  $\eta$  satisfies

$$\nabla \psi_t(\eta) = -P_t(\eta) = -\left( \mathbf{n}_t \times \sum_{i=1}^3 C_i \mathbf{d}_i - \omega_t \mathbf{n}_t \right). \quad (94)$$

Differentiating Eq. (93) with respect to  $\eta$  and obtain

$$\nabla \psi_t(\eta) = - \sum_{i=1}^3 \left[ (\mathbf{Z}_i \cdot \mathbf{n}_t) \nabla C_i + C_i \nabla (\mathbf{Z}_i \cdot \mathbf{n}_t) \right] - \frac{3}{A_t} \left( \text{vol}_t \nabla \omega_t + \omega_t \nabla \text{vol}_t \right). \quad (95)$$

The signed volume of the tetrahedron is  $\text{vol}_t = \frac{1}{3} A_t H_t$ . Consequently

$$\nabla \text{vol}_t = \frac{1}{3} A_t \nabla H_t = -\frac{1}{3} A_t \mathbf{n}_t. \quad (96)$$

Rearranging above formulation and get

$$\boxed{\nabla \omega_t = -\frac{1}{H_t} \sum_{i=1}^3 (\mathbf{Z}_i \cdot \mathbf{n}_t) \bar{C}_i (\bar{\mathbf{e}}_{i+1} + \bar{\mathbf{e}}_{i+2}),} \quad (97)$$

where  $H_t$  is the height of  $\eta$  toward  $t_j$ , which can also be computed as  $H_t = \mathbf{e}_1 \cdot \mathbf{n}_t$ . The formula for  $\nabla \omega_t$  differs slightly from that in [Ben-Chen et al. 2009], but we have verified that both are correct.

**6. Derivation of  $\mathbf{H}\phi_{\mathbf{v}_{j_1}}(\eta)$ .** Differentiating Eq. (88) directly yields

$$\boxed{\mathbf{H}\phi_{\mathbf{v}_{j_1}}(\eta) = - \sum_{t \in \mathcal{N}(\mathbf{v}_{j_1})} \frac{1}{2A_t} ([\mathbf{d}_1] \times \mathbf{J}(P_t)).} \quad (98)$$

The expression for  $\mathbf{J}(P_t)$  can be found in Eq. (92).

## C Supplementary Information for Experiments

### C.1 Anisotropic Matrices

Here, we provide some anisotropic matrices used in 2D deformation experiments. Note that  $\mathcal{A}(\theta, 1, \lambda) = \mathcal{A}(\theta + \frac{\pi}{2}, \lambda, 1)$ , so all rotation angles listed in the table are less than  $\frac{\pi}{2}$ .

$\theta$	$(\lambda_1, \lambda_2) = (1.0, 2.0)$	$(\lambda_1, \lambda_2) = (1.0, 4.0)$	$(\lambda_1, \lambda_2) = (2.0, 1.0)$	$(\lambda_1, \lambda_2) = (4.0, 1.0)$
0	$\begin{pmatrix} 1.0 & 0 \\ 0 & 2.0 \end{pmatrix}$	$\begin{pmatrix} 1.0 & 0 \\ 0 & 4.0 \end{pmatrix}$	$\begin{pmatrix} 2.0 & 0 \\ 0 & 1.0 \end{pmatrix}$	$\begin{pmatrix} 4.0 & 0 \\ 0 & 1.0 \end{pmatrix}$
$\pi/6$	$\begin{pmatrix} 1.25 & -0.4330127 \\ -0.4330127 & 1.75 \end{pmatrix}$	$\begin{pmatrix} 1.75 & -1.2990381 \\ -1.2990381 & 3.25 \end{pmatrix}$	$\begin{pmatrix} 1.75 & 0.4330127 \\ 0.4330127 & 1.25 \end{pmatrix}$	$\begin{pmatrix} 3.25 & 1.2990381 \\ 1.2990381 & 1.75 \end{pmatrix}$
$\pi/4$	$\begin{pmatrix} 1.5 & -0.5 \\ -0.5 & 1.5 \end{pmatrix}$	$\begin{pmatrix} 2.5 & -1.5 \\ -1.5 & 2.5 \end{pmatrix}$	$\begin{pmatrix} 1.5 & 0.5 \\ 0.5 & 1.5 \end{pmatrix}$	$\begin{pmatrix} 2.5 & 1.5 \\ 1.5 & 2.5 \end{pmatrix}$
$\pi/3$	$\begin{pmatrix} 1.75 & -0.4330127 \\ -0.4330127 & 1.25 \end{pmatrix}$	$\begin{pmatrix} 3.25 & -1.2990381 \\ -1.2990381 & 1.75 \end{pmatrix}$	$\begin{pmatrix} 1.25 & 0.4330127 \\ 0.4330127 & 1.75 \end{pmatrix}$	$\begin{pmatrix} 1.75 & 1.2990381 \\ 1.2990381 & 3.25 \end{pmatrix}$

## C.2 Computation of distortion

We compute the isometric distortion  $E_{\text{iso}}$ , conformal distortion  $E_{\text{conf}}$  and area distortion  $E_{\text{area}}$  as follows:

$$E_{\text{iso}} = (\sigma_1 - 1)^2 + (\sigma_2 - 1)^2, \quad (99)$$

where  $\sigma_1$  and  $\sigma_2$  are the two singular values of the Jacobian matrix of the deformation map. The conformal distortion evaluates the deviation from angle preservation and is expressed as

$$E_{\text{conf}} = \frac{\sigma_1}{\sigma_2} + \frac{\sigma_2}{\sigma_1} - 2, \quad (100)$$

which vanishes if and only if  $\sigma_1 = \sigma_2$ . Finally, the area distortion quantifies the deviation from unit area scaling and is given by

$$E_{\text{area}} = |\sigma_1 \sigma_2 - 1|. \quad (101)$$

The metrics are computed as the average over all pixels in the input image.

## References

Mirela Ben-Chen, Ofir Weber, and Craig Gotsman. 2009. Variational harmonic maps for space deformation. *ACM Transactions on Graphics* 28, 3 (2009), 34.

Yaron Lipman and David Levin. 2009. Derivation and analysis of Green coordinates. *Computational Methods and Function Theory* 10, 1 (2009), 167.

Yaron Lipman, David Levin, and Daniel Cohen-Or. 2008. Green coordinates. *ACM Transactions on Graphics* 27, 3 (2008), 78.

Élie Michel, Alec Jacobson, Siddhartha Chaudhuri, and Jean-Marc Thiery. 2025. Variational Green and biharmonic coordinates for 2D polynomial cages. *ACM Transactions on Graphics* 44, 4 (2025), 76:1–76:20.

Laurent Schwartz. 1966. *Théorie des distributions*. Hermann.

Masataka Urago. 2000. Analytical integrals of fundamental solution of three-dimensional Laplace equation and their gradients. *Transactions of the Japan Society of Mechanical Engineers Series A* 66, 642 (2000), 254–260. in Japanese.